The discriminatory power of the T cell receptor

Anna Huhn[1], Daniel B. Wilson[1,2], P. Anton van der Merwe[1], Omer Dushek[1¶]

[1]Sir William Dunn School of Pathology, University of Oxford, OX1 3RE, Oxford, UK
[2]Boston University, Department of Mathematics and Statistics, Boston, MA 02215
[¶]Corresponding author (omer.dushek@path.ox.ac.uk)

Abstract

T cells use their T-cell receptors (TCRs) to discriminate between lower-affinity self and higher-affinity non-self pMHC antigens. The strength of this discrimination and the mechanisms that produce it remain controversial. Although a large number of mouse and human TCRs have now been characterised, they have not been used to precisely quantitate discrimination. Here, we systematically quantify the discrimination of TCRs using a discrimination power (α). Early influential studies on three mouse TCRs suggested that discrimination was nearly perfect ($\alpha \sim 9.0$). In striking contrast, our analysis of published data on other mouse and human TCRs, and more recent data on the original mouse TCRs, produced significantly lower discrimination ($\alpha = 2.0$). Although not perfect, the discriminatory power of TCR was greater than that of conventional receptors such as cytokine receptors, GPCRs, RTKs, and CARs ($\alpha \leq 1$). The revised discriminatory power of the TCR is readily explained by a kinetic proof-reading mechanisms, and accounts for the ability of low affinity self-antigens to stimulate autoimmune and anti-tumour T cell responses.
(**155 words**)

Introduction

T cells initiate and regulate adaptive immune responses by using their T cell receptors (TCRs) to recognise peptide antigens bound to major histocompatibility complexes (pMHCs) on antigen-presenting-cells (APCs). Importantly, T cells are not normally activated by APCs that present only self-protein derived pMHCs but become activated when these APCs express even a few non-self-protein derived pMHCs. This ability to discriminate between self and non-self pMHCs is the basis of adaptive immunity and although extensively studied, the degree of discrimination and the underlying mechanisms are debated (1–3)

Early work using three mouse TCRs (4–9) suggested that T cells can exhibit near perfect discrimination based on the TCR/pMHC unbinding rate (k_{off}) or the dissociation constant (K_D) (Fig. 1A). K_D is a reasonable proxy for k_{off} because on-rates (k_{on}) vary much less than k_{off} (10, 11). Using T cells from the OT-I, 3L.2, and 2B4 transgenic TCR mice, it was shown that subtle changes to their cognate peptides, which apparently produced modest 3-5-fold changes in K_D, abolished the T cell response even when increasing the peptide concentration (4–9). This was also reproduced with T cells stimulated by plate-coated recombinant pMHC in isolation (12), suggesting that discrimination is intrinsic to T cells and the TCR. Although these mouse TCRs remain integral to studies of antigen discrimination, a number of other mouse and human TCRs have now been characterised and these do not display the same features. Qualitative inspection of these other TCRs shows that they display a more gradual loss of the response as the affinity is decreased (e.g. 1G4 (10)). Moreover, multiple lines of evidence have suggests that T cells can respond to lower affinity antigens in clinical settings. For example, T cells specific for self antigens have been implicated in autoimmune diseases and in anti-tumour responses. The affinities of their TCRs for self-antigen pMHC are lower than reported for T cells directed against foreign pMHC (13, 14). Furthermore, increased expression of self-antigens have been implicated in T cell-mediated autoimmune diseases (15, 16). Therefore, there is an apparent discrepancy between the original mouse TCR data suggesting near perfect discrimination and data emerging from the study of other TCRs.

The molecular mechanisms underlying discrimination also remain unclear. It was recognised early on that a receptor occupancy model, whereby the T cell response is proportional to the number of bound TCR, cannot explain TCR discrimination. In this model, increasing the peptide concentration by 3-5-fold is predicted to compensate for a 3-5-fold decrease in affinity, which is not observed experimentally (1, 17). Instead, a kinetic proofreading (KP) mechanism was proposed to explain discrimination (18, 19). However, subsequent studies revealed that T cells exhibit remarkable ligand sensitivities and can respond to even a single pMHC (20, 21). Given that the KP mechanism has a trade-off between discrimination and sensitivity, it was unable to simultaneously explain the near perfect discrimination and high ligand sensitivity (1) unless it was augmented with additional mechanisms, such as feedbacks (22–34).

The TCR is considered unique among surface receptors because unlike other receptors, such as hormone, growth factor, or cytokine receptors that are germline encoded and have defined ligands, the TCR is generated by recombination and can bind >100,000 ligands with a spectrum of affinities (35, 36). Although the TCR is clearly qualitatively unique, it is unclear whether it is quantitatively unique in its ability to perform ligand discrimination based on affinity or off-rate. This is challenging to investigate because other receptors typically bind one or few ligands and therefore, their discrimination abilities have not been investigated. Quantitative comparisons across receptor families can provide insights into the mechanism of discrimination.

Here, we performed a systematic analysis of ligand discrimination by taking advantage of studies that used natural or synthetically engineered receptor/ligands. We first introduce the discrimination power pa-

rameter (α) as a quantitative measure of ligand discrimination. Using this measure, we quantified the near-perfect discrimination using early mouse TCR studies ($\alpha \sim 9.0$), but found significantly lower discrimination powers for subsequent studies of mouse and human TCRs ($\alpha = 2.0$). Importantly, this discrimination power was higher than the discrimination power obtained for other (non-TCR) receptors ($\alpha \leq 1.0$). Therefore, the TCR exhibits enhanced discrimination compared to other receptors, and this level of discrimination can readily be explained by kinetic proofreading.

Results

Quantifying ligand discrimination with a discrimination power (α)

The strength of ligand discrimination can be defined by the ability of the TCR to amplify changes in ligand affinity (or off-rate) into larger changes in ligand potency, which is the concentration of ligand required to produce a given level of response. To quantitatively compare studies that used different TCR/pMHC affinity ranges and different measures of T cell activation, it was important to identify a discrimination measure that was robust to these differences. We noted that plots of ligand potency (P) over $\mathrm{K_D}$ often displayed a linear relationship on logarithmic axes. This suggested a power law relationship (i.e. $P = 10^C(\mathrm{K_D})^\alpha$) whereby the power ($\alpha$) is the slope on logarithmic axes (i.e. $\log(P) = C + \alpha\log(\mathrm{K_D})$). This suggested that α, which is independent of scale and dimensionless, can be a robust discrimination measure. The intercept, C, can be interpreted as measure of ligand sensitivity but unlike the power, it would be dependent on scale and would have dimensions making it difficult to compare between studies. We therefore, focused on α.

To illustrate the role of α in discrimination, we simulated the T cell response (R) over ligand concentration (L) using a saturating function ($R = L/((K_\mathrm{D})^\alpha + L)$ with different values of α representing 3 levels of discrimination (Fig. 1B). When $\alpha = 9$, a small 4-fold increase in $\mathrm{K_D}$ (from 1 to 4) nearly abolishes the response whereas when $\alpha = 1$, a 4-fold increase in $\mathrm{K_D}$ can be compensated for by a 4-fold increase in ligand concentration. Mechanistically, a receptor occupancy model produces $\alpha = 1$ (termed baseline discrimination) whereas additional mechanisms such as KP are required to produce $\alpha > 1$ (termed enhanced discrimination). We calculated the concentration of ligand producing a response of 0.5 (P, ligand potency) and plotted it over $\mathrm{K_D}$ (Fig. 1C). As expected, we observed linear relationships on logarithmic axes with the slope being equal to the discrimination power (α). Moreover, we found that the slope was robust to the precise definition of ligand potency so that the same slope was produced when using a different response threshold (e.g. 0.25 or 0.75, instead of 0.5, not shown). Therefore, the discrimination power (α) can be inferred from the slope of a logarithmic potency plot. We defined two ranges of enhanced discrimination ($\alpha > 1$) with α values in the range of 1-5 as good discrimination whereas values > 5 as near-perfect discrimination. We next sought to determine the value of α from published studies.

Analysis of the early mouse TCR data suggests near-perfect discrimination powers

We began our study by applying our analysis to the original mouse TCR data, which has been highly influential on our current understanding of TCR discrimination (Fig. 2). In the case of the OT-I TCR (Fig. 2A, top), the T cell response was measured by the percent of target cells killed (4) and we defined potency as the ligand concentration producing 10% lysis ($\mathrm{P_{10}}$) in order to include the E1 peptide variant. The original binding data was provided in a subsequent study using surface plasmon resonance (SPR) (6). As expected,

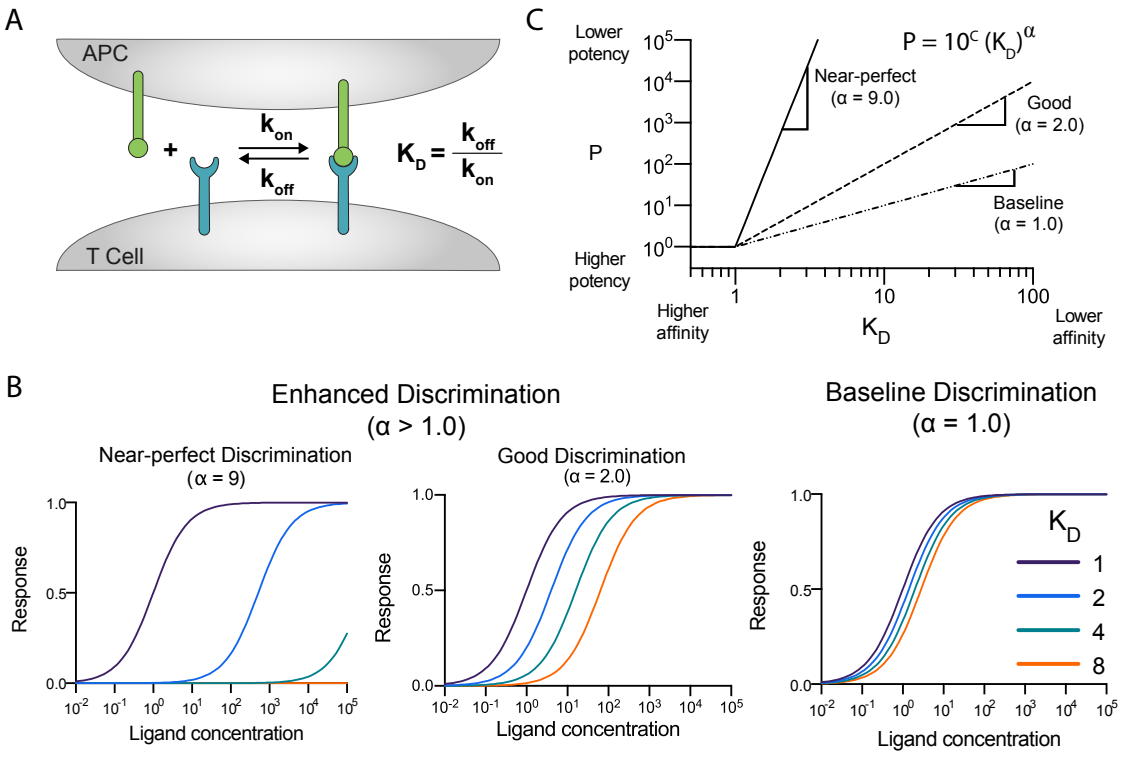

Figure 1: **Quantifying ligand discrimination with a discrimination power (α).** A) TCR/pMHC binding schematic. B) Simulated T cell response over the ligand concentration for four representative ligands that bind with the indicated affinity. Examples of T cell response profiles are shown for enhanced near-perfect discrimination ($\alpha \geq 5$, left), enhanced good discrimination ($1 < \alpha < 5$, middle), and baseline discrimination ($\alpha = 1$, right). C) The concentration of ligand producing a response of 0.5 (P, potency) is plotted over K_D. The discrimination power (α) is the slope on the log-log plot.

plotting potency over K_D produced a steep slope ($\alpha = 10.5$) with near-perfect discrimination (Fig. 2A, bottom). This is a result of the E1 peptide variant having a 5×10^6-fold lower potency despite binding with only a 3.5-fold lower affinity compared to the wild-type OVA peptide. We found similar values of α (12, 18, and > 5.1) when using functional data from other studies (5, 25, 37) (Table S1 ID 1-4).

Similar to OT-I, the original 3.L2 (7, 8) (Fig. 2B) and 2B4 (9) (Fig. 2C) data also produced perfect discrimination powers. In the case of 3.L2, we plotted potency over k_{off} instead of K_D because k_{on} was different between pMHCs (8) (Fig. 2B, bottom). A significant correlation was only produced for the 3L.2 TCR, which is partly a result of fewer data points for the OT-I and 2B4 TCRs. Notwithstanding this limitation, the analysis confirmed that the original mouse TCR data produced large powers consistent with perfect discrimination.

Revised data for the original mouse TCRs produce lower discrimination powers

The OT-I, 3L.2, and 2B4 transgenic mice have been instrumental in advancing our understanding of T cell immunity. As such, substantial data has been generated relating to these TCRs over the years, including new

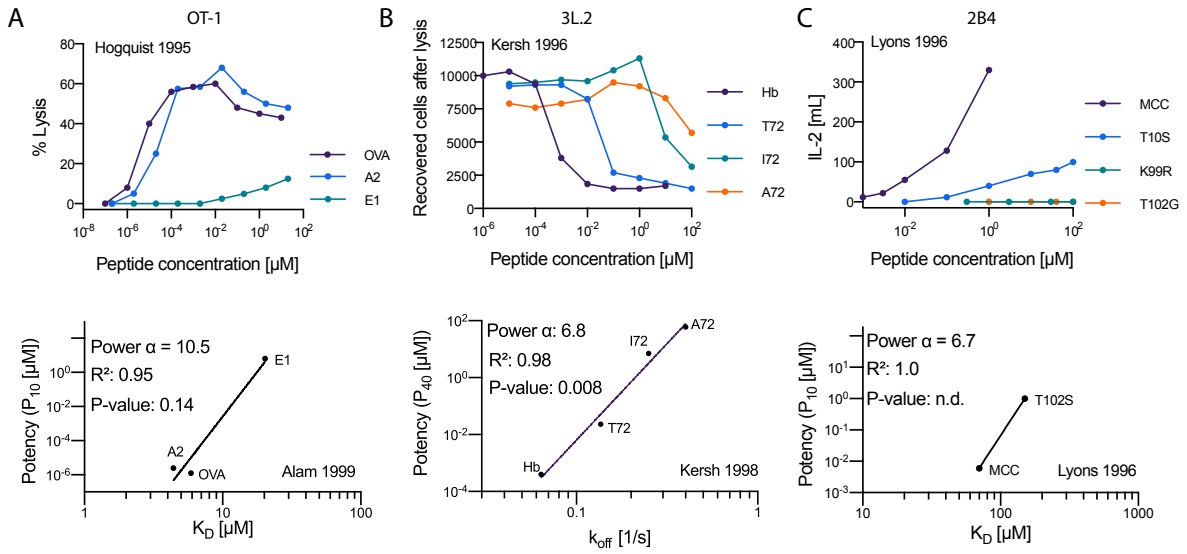

Figure 2: **Original mouse TCR data suggests near-perfect discrimination.** T cell dose-responses over the concentration of the indicated peptide ligand (top row) and potency/affinity plots (bottom row) for the A) OT-I, B) 3L.2, and C) 2B4 mouse TCRs. The discrimination power (α) is indicated and corresponds to the slope on the log-transformed data. Additional information on each data is provided in Table S1 (ID: 2 (OT-I), 11 (3L.2), and 14 (2B4)).

measurements of TCR/pMHC binding that have not been used to quantify discrimination.

In the case of the OT-I TCR, the original SPR data had unusual biphasic binding with unusually slow off- and on-rates for a TCR (6). More recently, two studies have found the usual monophasic binding with fast kinetics for OT-I binding the wild-type OVA peptide (38, 39) and no detectable binding for the E1 peptide variant (38). This latter observation is important because the high discrimination power in the original data was predicated on this E1 peptide binding with just an 3.5-fold lower affinity (Fig. 2A). Without binding data for the E1 peptide, we were unable to use the original potency data to produce a revised discrimination power. Instead, we took advantage of four different peptide variants for which the T cell activation and OT-I TCR binding properties were characterised by Daniels et al (40) and Stepanek et al (38). We found a significant correlation between potency and K_D that produced an appreciably lower discrimination power of 2.1 (Fig. 3A).

In the case of the 3.L2 TCR, revised SPR data for the original 4 peptide variants showed a wider variation in k_{off} and K_D than originally reported (41). Given that k_{off} could not be accurately determined for 2 of the 4 pMHCs in the revised measurements, we re-plotted the original potency data over the revised K_D values, and as for the OT-I TCR, we found a significant correlation with an appreciably lower power of 3.2 (Fig. 3B). Similarly, re-plotting the 2B4 TCR potency data over revised SPR data (42) produced an appreciably lower discrimination power of 2.8 (Fig. 3C). Although we were only able to include two data points for this calculation when using the original potency data, we identified two additional studies that contained revised SPR and functional data for the 2B4 TCR (36, 43). These produced significant correlations between potency and K_D resulting in lower discrimination powers of 2.3 and 0.95 (Table S1 ID 18 and 19).

We collated the discrimination powers for the OT-I, 3L.2, and 2B4 TCRs finding a mean value of $\alpha \sim 9$

when using the original SPR data and $\alpha = 2.2$ when using revised data (Fig. 4A, Table S1 ID 1-19). This analysis highlighted that the discrimination power of these TCRs may be lower than previously thought.

Analyses of other mouse and human TCRs also produce lower discrimination powers

The analysis in the previous two sections have highlighted a discrepancy in the discrimination power of the OT-I, 3L.2 and 2B4 mouse TCRs. It was not possible to resolve the discrepancy using these TCRs because of the limited data underlying each calculated α, which meant that most were not significant, and the limited number of independent estimates of α. Although not used to inform quantitatively on discrimination, many other mouse and human TCRs have been characterised over the past two decades. Therefore, we applied our analysis to calculate discrimination powers for these other TCRs.

For a TCR to be included in this study, a dose-response had to have been performed so that a measure of ligand potency can be determined and in addition, monomeric TCR/pMHC binding data (K_D or k_{off}) had to be available. We used studies that relied on different peptides that bound a single TCR, studies that relied on multiple TCRs that bound the same peptide, or studies that relied on a combination of both. We generated 51 potency plots (Fig. S2, S3, S4) and extracted the discrimination power (Table S1 ID 20-70). As representative examples, we show the dose-response and corresponding potency plots for the mouse B3K506 TCR (Fig. 3D) and the human 1G4 TCR (Fig. 3E) and 1E6 TCR (Fig. 3F). These TCRs produced discrimination powers ranging from 1.2 to 2.9. Moreover, other mouse (P14, B3K508, AH1 specific) and human (1E6, gp100 specific, ILA1, gliadin specific, LC13, gag-specific, and MEL5) TCRs had discrimination powers in a similar range (Fig. 4B). Thus, we found similar discrimination powers for the original mouse TCRs when using revised data to other mouse and human TCRs and these discrimination powers were significantly lower than those suggested by the original mouse TCR data (Fig. 4A). We therefore conclude that the discrimination power of the TCR is significantly lower than previously believed.

The discrimination power is similar for different T cell responses but depends on coreceptors and the antigen presentation surface

The collated discrimination powers used for the analysis (Fig. 4A) were derived from diverse studies that used either $CD4^+$ or $CD8^+$ T cells measuring different T cell responses when antigen is presented on APCs with wild-type CD4/CD8 co-receptor interactions. We took advantage of this diversity to explore whether there were any differences between conditions.

We first grouped the discrimination powers based on whether $CD4^+$ or $CD8^+$ T cells were used and found no difference (Fig. 4C). We also examined the discrimination power based on the T cell response that was measured in each study finding broadly similar discrimination powers (Fig. 4D). This is consistent with a TCR-proximal mechanism of antigen discrimination (44, 45) that has a similar threshold for different T cell responses (46–48).

We next examined whether the presence of CD4/CD8 co-receptors had an impact on discrimination. It is well established that they can impact T cell sensitivity to antigen (49, 50) but less is known about their contribution to discrimination. We identified studies where co-receptor binding was abolished and contained information to calculate a discrimination power (45, 51, 52). We found a significant increase in the discrimination power when co-receptors action was impaired using all data (Fig. 4E) or when we limited

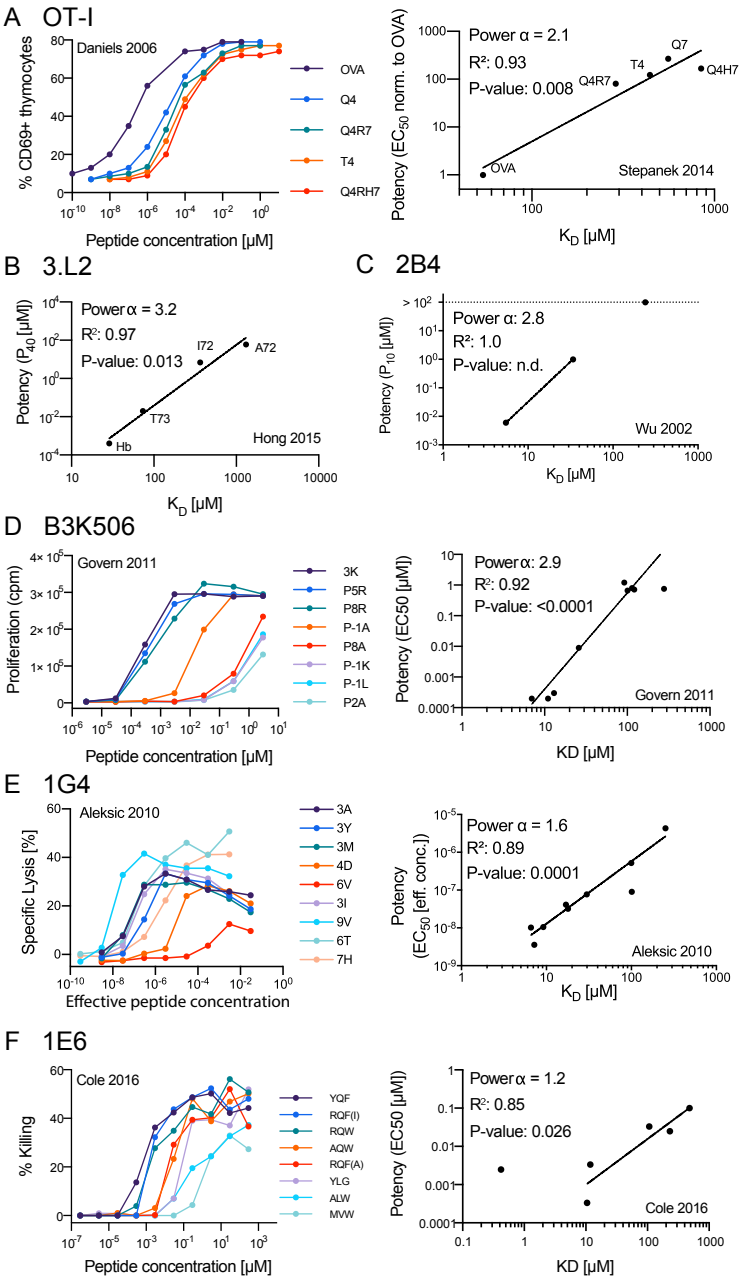

Figure 3: **Revised analyses of the original mouse TCRs, and analyses of other mouse and human TCRs, reveal modest discrimination powers.** A-C) Revised analysis of the original murine TCRs by using A) new functional and SPR binding data for OT-I, B) new SPR binding data for 3.L2, and C) new SPR binding data for 2B4. D-F) Examples of analyses of other mouse (B3K506) and human (1G4, 1E6) TCRs. We note that for the 1E6 TCR, the highest affinity peptide with $K_D < 1$ μM was excluded because it saturated the T cell response and would have led to artificially lowering the estimate of α (see Methods for inclusion and exclusion criteria). Additional information on each panel is provided in Table S1 (ID: 5 (OT-I), 13 (3L.2), 17 (2B4), 23 (B3K506), 38 (1G4), and 42 (1E6)).

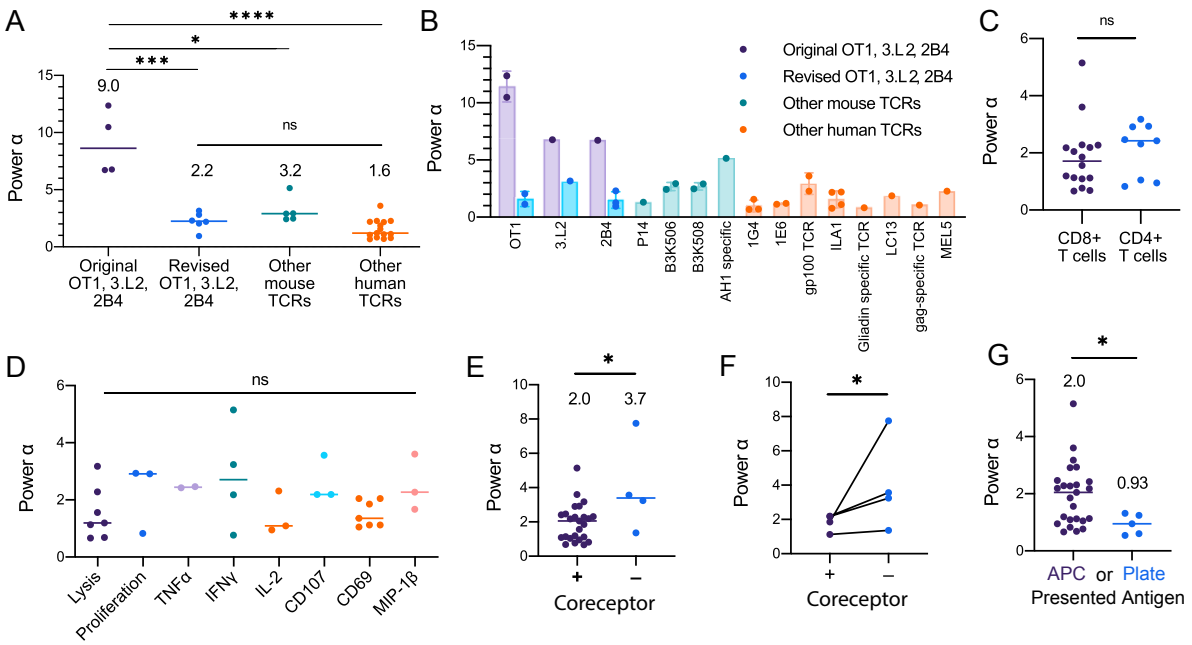

Figure 4: **Statistical analyses across multiple TCR/pMHC systems confirm lower discrimination powers that can be modulated by coreceptors and the antigen presentation surface.** A) Comparison of discrimination powers from the original mouse TCR data (n=4), revised mouse TCR data (with revised SPR data, n=6), and other mouse (n=5) and human (n=15) TCRs. Statistical significance was determined using one-way ANOVA. B) The discrimination powers shown in panel A parsed into the indicated TCR/pMHC system. C) Comparison between $CD4^+$ and $CD8^+$ T cells. D) Comparison between different T cell responses. E) Comparison between conditions with and without the CD4/CD8 co-receptors. F) Comparison as in E but for paired data (i.e. where both conditions were present in the same study). G) Comparison between the use of APCs or artificial plate surfaces to present antigens. Data with antigen presented on plates or without coreceptors were not included in any other analyses shown in panels A-D and analyses in C-G is based on combining the revised OT-1, 3.L2, and 2B4 data, other mouse TCRs, and other human TCRs that together produce a mean value of $\alpha = 2.0$ (95% CI of 1.5 to 2.4). Complete list of all 70 calculated powers can be found in Table S1.

the comparison to paired data (Fig. 4F). This suggests that co-receptors improve T cell sensitivity to antigen but at a cost to their discrimination power.

All studies included in our analysis so far have relied on the presentation of antigen ligands on APCs. We found a number of studies, including previous work from our laboratory, that relied on reductionist systems where recombinant pMHC is presented in isolation on plates (e.g. biotinylated pMHC immobilised on streptavidin-coated plates (10, 11, 47, 53, 54)). To assess the impact of artificial presentation, we quantified discrimination powers from these studies finding that α decreased significantly from 2.0 on APCs to 0.93 when presented on artificial surfaces (Fig. 4G). This result suggests that other factors, beyond TCR/pMHC interactions, may contribute to enhancing discrimination.

In summary, the discrimination power of the TCR appeared to be similar for both $CD4^+$ and $CD8^+$ T cells and their different responses but was significantly reduced by the action of coreceptors or when antigen was presented on plates.

The ligand discrimination power of the TCR is higher than conventional surface receptors

The observation that the TCR exhibits good discrimination that is only modestly above the baseline predicted by the receptor occupancy model raises the important question of whether the TCR is unique in its ligand discrimination abilities. The TCR is clearly qualitatively unique because, unlike other receptors that evolved to bind one (or few) defined ligand(s), it can bind large numbers of different ligands that it has never previously encountered (35, 36). However, the discriminatory power of the TCR has not previously been compared with other receptors.

Efforts to understand the basic function of receptors and to exploit them for therapy have generated dose-response data using both natural and also synthetic receptors and/or ligands that bind with different affinities. This data offered the opportunity to estimate the discrimination powers of Cytokine receptors, RTKs, GPCRs, and chimeric antigen receptors (CARs) (Fig. 5).

Cytokine receptors transduce signals by ligand-induced dimerisation of receptor subunits. This brings their associated Janus kinases (JAKs) into proximity ultimately leading to the activation of signal transducer and activator of transcription (STATs). We identified 5 studies that produced ligands with mutations that modified binding to either one or both receptor subunits and either reported potency or provided dose-response curves from which potency can be extracted (55–59). As an example, Moraga et al (56) generated IL-13 variants with mutations that resulted in a broad range of affinities to the IL-13Rα1 subunit but maintained the wild-type interface, and hence the same affinity, to the IL-4Rα subunit. By measuring cellular responses, such as upregulation of CD86 on monocytes, dose-response curves were generated for each IL-13 variant allowing us to determine ligand potency. As expected, we observed a significant correlation between potency and K_D (Fig. 5A) and interestingly, the fitted discrimination power was only $\alpha = 0.44$. We repeated the analysis for each study (Table S2 ID 1-13). In studies that included ligands with mutations to both receptor interfaces, we plotted potency over the product of the dissociation constants to each interface since this serves as an estimate of the overall affinity (i.e. $K_D^1 \times K_D^2$). Collating these studies revealed a mean discrimination power of $\alpha = 0.66$ (Fig. 5F).

Like cytokine receptors, RTKs transduce signals by ligand-induced dimerisation which brings their cytoplasmic kinase domains into proximity to facilitate trans-auto-phosphorylation. We identified two potential studies to include in the analysis (60, 61). Ho et al (60) generated stem cell factor (SCF) ligand variants to the RTK c-Kit. SCF induces c-Kit dimersation by binding to c-Kit with one interface and binding to another SCF with a different interface generating SCF/c-Kit homodimers. Four SCF variants were used in detailed dose-response assays measuring phosphorylation of ERK (Fig. 5B, left) and AKT (not shown here) in mouse mast cells. Given that the SCF variants included mutations impacting both c-Kit binding and SCF homodimersation, we plotted potency over the product of the dissociation constants for each interface finding a significant correlation for ERK (Fig. 5B, right) and AKT (Fig. S5 ID 16). The discrimination powers were 0.83 for ERK and 0.88 for AKT. A significant correlation was not observed for the second study using EGFR (Table S2 ID 14) and therefore, we estimated the mean for RTK based on the c-Kit data to be $\alpha = 0.86$ (Fig. 5F).

Although multiple ligands for a given GPCR have been described, they often bind at different GPCR sites to stabilise different receptor conformations and hence transduce qualitatively different signals. Therefore, ligand affinity may not correlate to functional potency. Instead, we focused on identifying studies that used ligands that were confirmed to bind to the same interface with different affinities. As an example, Sykes et al (62) used 7 agonists to the muscarinic M_3 receptor and confirmed they all bound to the same interface using a binding competition assay. Using titrations of each ligand, they examined the binding of GTPγS

to CHO-M_3 membrane as a measure of response (Fig. 5C, left). Plotting ligand agonist potency over K_D produced a significant correlation with a discrimination power of $\alpha = 0.55$ (Fig. 5C, right). We found a similar discrimination power when using a different measure of response (Ca^{2+} mobilisation from CHO-M_3 cells) from the same study and moreover, similar discrimination powers in other studies investigating the A2A receptor (63) and the chemokine receptors CXCR4 (64) and CXCR3 (65) (Table S2 ID 17-24). Collating these studies revealed a mean discrimination power of $\alpha = 0.76$ (Fig. 5F).

Chimeric antigen receptors (CARs) are therapeutic receptors often expressed in T cells that fuse an extracellular antigen recognition domain to an intracellular signalling domain (often the ζ-chain from the TCR). The optimisation of CAR-T cell therapy has focused on modifying different components of the synthetic receptor, including the CAR/antigen affinity. We took advantage of these studies to determine the discrimination power of CARs. As an example, Chmielewski et al (66) generated a panel of CARs that bind the ErbB2 receptor (target antigen) with different affinities. CAR-T cells were stimulated with a titration of recombinant ErbB2 and their ability to produce the cytokine IFNγ was used to measure T cell responses (Fig. 5D, left). We found a significant correlation between potency and K_D with a discrimination power of $\alpha = 0.52$ (Fig. 5D, right). Similar results were observed using a different ErbB2 CAR (67) and a DNA-based CAR (68) (Table S2 ID 25-28). Together, we found a mean discrimination power of $\alpha = 0.94$ (Fig. 5F).

Lastly, antigen discrimination has also been reported for the B cell receptor (BCR), which shares many structural and functional features with the TCR. Although several studies have investigated BCR ligand discrimination, we identified only a single study with the requisite dose-response curves that are necessary to quantify the discrimination power. Batista et al (69) used two lysozyme-specific BCRs (HyHEL10 and D1.3) to perform dose-response curves to wild-type or mutated lysozyme variants measuring the production of the cytokine IL-2 (Fig. 5E, left). We estimated potency directly from the dose-response curves and found a significant correlation with k_{off} (Fig. 5E, right). In contrast to the other receptors where $\alpha \leq 1$, we found the discrimination power for both HyHEL10 and D1.3 BCRs to be > 1 (mean of $\alpha = 1.3$, Fig. 5F).

In summary, we found similar discrimination powers that were lower than but near 1 for Cytokine receptors, RTKs, GPCRs, and CARs and as a group, these other receptors exhibited significantly lower discrimination compared to the TCR (Fig. 5F). Therefore, the enhanced discrimination power of the TCR ($\alpha > 1$) is higher than the discrimination power achieved by other surface receptors ($\alpha \leq 1$), suggesting that the TCR is both qualitatively and quantitatively unique among surface receptors.

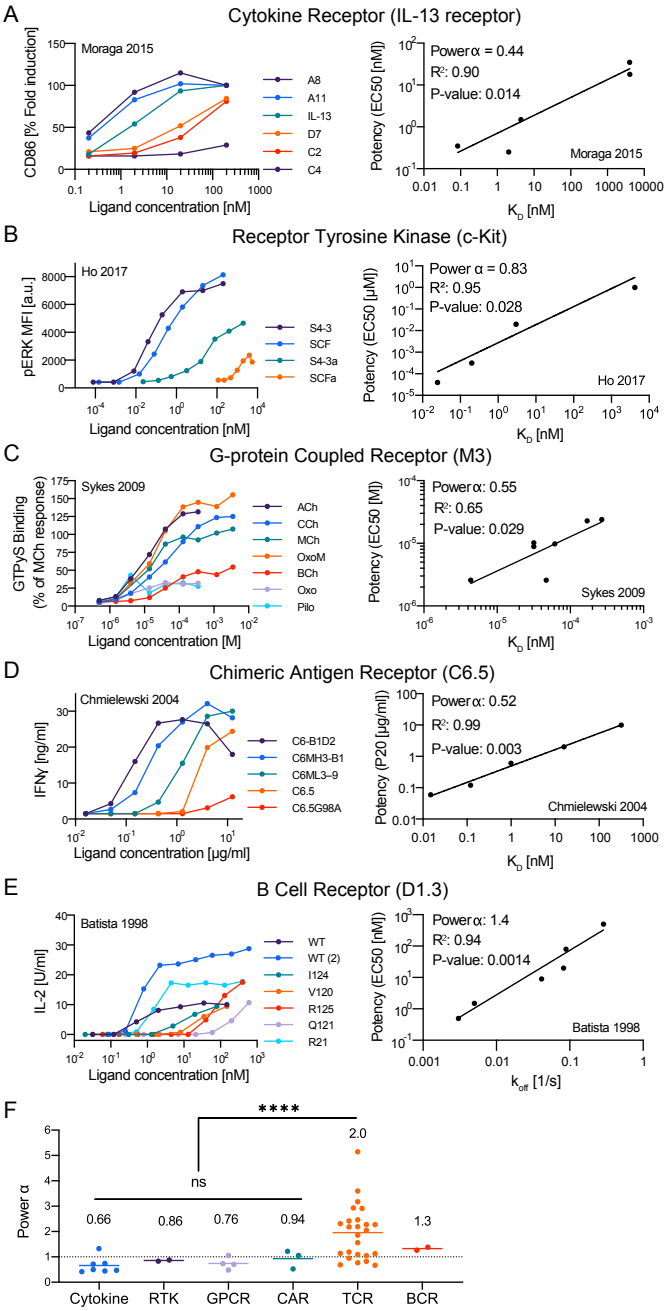

Figure 5: **The discrimination power of the TCR is higher than other surface receptors.** A-E) Representative dose-response (left column) and potency over K_D or k_{off} (right column) for A) the IL-13 cytokine receptor, B) the c-Kit receptor tyrosine kinase, C) the muscarinic M_3 G-protein coupled receptor, D) ErbB2-specific chimeric antigen receptors, and E) a lysozyme-specific B cell antigen receptor (D1.3). F) Discrimination powers from all studies included in our analysis (Table S1 for TCRs and Table S2 for other receptors). Comparisons within other receptors (cytokine receptors, RTKs, GPCRs, and CARs) and between other receptors and the TCR was performed using a one-way ANOVA and a non-paired t-test, respectively. The BCR was not included in statistics. Additional information on each panel is provided in Table S2 (ID: 5 for panel A, 15 for B, 20 for C, 25 for D, and 29 for E).

Kinetic proofreading can simultaneously explains TCR sensitivity and discrimination

The kinetic proofreading (KP) model was initially proposed as a phenotypic (or operational) model to explain how TCRs were able to discriminate between the abundant low affinity self pMHC and rare high affinity foreign pMHC (18). The model proposes that a series of N biochemical steps, each with rate k_{p}, must take place between ligand binding (step 0) and a productive TCR signal (step N) (Fig. 6A). Although the model could in principal explain high levels of discrimination, a trade-off in the KP mechanism meant that this level of discrimination came at a cost to antigen sensitivity (23).

To illustrate this, we systematically varied the KP parameters and calculated a measure of TCR sensitivity and discrimination (Fig. 6B). To determine TCR sensitivity, we determined whether the number of productively signalling TCRs is above a threshold, T, for a single agonist pMHC (coloured red if true). To determine TCR discrimination, we determined whether the number of productively signalling TCRs was below the same threshold T for a pMHC that was expressed at 10,000-fold higher concentration but bound with a Δ-fold lower affinity (coloured blue if true). To reproduce perfect discrimination powers ($\alpha = 9.0$), we used $\Delta = 2.8$ (e.g. OVA vs E1 in the original mouse TCR data) and to produce good or baseline discrimination, we used $\Delta = 100$ or $\Delta = 10,000$, respectively (see Supplementary Information). The resulting heat maps showed the trade-off, revealing that KP parameters that gave the required sensitivity were incompatible with near-perfect discrimination and vice versa (Fig. 6B, left). In contrast, KP parameters could produce the required sensitivity and the level of discrimination typical of TCRs (Fig. 6B, middle). In this case, we found that the minimum number of steps (N) and the fastest proofreading rate (k_{p}) consistent with both sensitivity and discrimination were 2 and 0.5, respectively.

We next used these KP parameter values to simulate the dependence of potency on k_{off} (equivalent to $\mathrm{K_D}$ when k_{on} is constant), and found that they produced similar discriminatory powers to those observed in our analysis, namely a slope of $\alpha = 2.0$ (Fig. 6C). We note that $\alpha \approx N$ in this standard KP mechanism provided that α is estimated using the linear phase of the logarithmic potency plot (i.e. away from the higher affinity where potency saturates). Lastly, we examined the impact of the threshold parameter on the minimum number of steps required to explain simultaneously sensitivity and discrimination, finding that $N \approx 2.0$ can explain good discrimination over a wide range of thresholds (Fig. 6D). Therefore, we conclude that the KP mechanism can explain both sensitivity and good discrimination, and moreover, can do this using fast proofreading times (e.g. $\tau_{\mathrm{kp}} = N/k_{\mathrm{p}} = 4.0$ s in our example), which is consistent with the observed speed of antigen recognition (1).

Discussion

The quantitative analysis we have carried out has revealed that the TCR exhibits a good discrimination power of $\alpha = 2.0$. The original mouse TCR data suggested much higher near-perfect discrimination with $\alpha \sim 9.0$. The discrepancy with other mouse and human TCRs is likely a result of errors in the original SPR affinity/kinetic measurements, which in the case of OT-I for example, showed unusual biphasic binding (6) (see Pettmann et al for discussion (70)). This conclusion is supported by our observation that revised potency over affinity data for OT-1, and revised affinity data for 3L.2 and 2B4 using the original potency data, produced lower discrimination powers, similar to values obtained for many other TCRs (Fig. 4A,B). Moreover, in a separate study not included in the present analysis, we confirmed this lower level of discrimination using primary human $\mathrm{CD8^+}$ T cells finding $\alpha = 1.8 - 2.1$ (70).

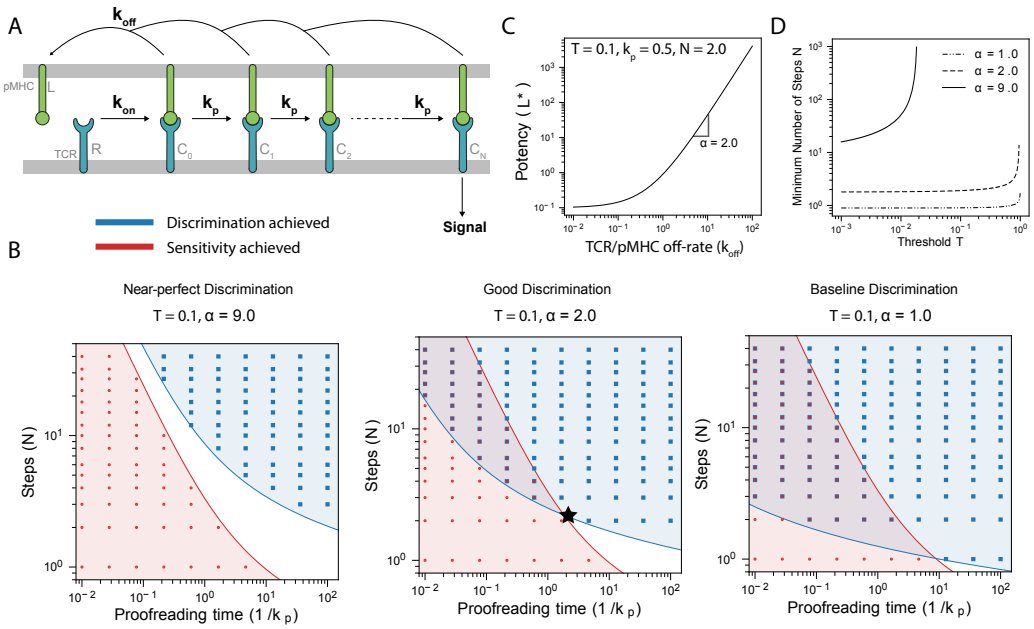

Figure 6: **Kinetic proofreading can readily explain the TCR discrimination power and sensitivity.** A) Schematic of the KP model. B) Systematic variations of the number of steps (N) and the proofreading time ($1/k_{\mathrm{p}}$) indicating whether the constraints of sensitivity (red) and discrimination (blue) are met for different levels of discrimination (near perfect, good, and baseline). Results using discrete stochastic simulations (dots) or deterministic calculations (continuous colours) are shown. The minimum number of steps to explain both discrimination and sensitivity is indicated for good discrimination (black star at $N \approx 2$, $k_{\mathrm{p}} \approx 0.5$ s^{-1}). C) Potency over k_{off} using KP parameters consistent with sensitivity and good discrimination. D) Minimum number of KP steps required to explain both sensitivity and the indicated level of discrimination over the threshold parameter. See Supplementary Information for deterministic and stochastic model calculations, including quantitative definitions of discrimination and sensitivity.

Although ligand potency often correlates with $\mathrm{K_D}$, there are published examples where T cells fail to respond to pMHCs that can bind their TCR. In one example, a structural explanation was provided for a pMHC that could bind the TCR but could not activate T cells; it exhibited an unusual docking geometry that prevented co-receptor binding (71). In another example, it was suggested that modulation of k_{off} by mechanical force contributed to discrimination (72, 73). Finally, in a third example, it was shown that the 2D TCR/pMHC binding parameters predicted the T cell response more accurately compared to the 3D binding parameters (74). However, this was based on the OT-I TCR system and relied on the early inaccurate SPR data, which was the only data available at the time. Interestingly, a different study found that the 2D and 3D binding parameters for the 1E6 TCR were equally accurate at predicting the T cell response (75). Taken together, these studies suggest that the enormous structural diversity of TCRs and their pMHC ligands means that there are likely to be exceptions where 3D binding properties do not correlate with potency. This may explain the lack of correlation between potency and $\mathrm{K_D}$ reported in a subset of the studies included in our analysis (Table S1).

The data in this analysis could not identify unique KP parameters, however, we were able to identify the minimum number of KP steps (two), which produced a short proofreading time-delay (4 s), that produce a high ligand sensitivity and a good discrimination power. The small number of steps is consistent with recent

reports suggesting that there are 2.7 steps (70, 76). The short proofreading time-delay is consistent with the high speed reported for antigen recognition (1, 77). The molecular mechanisms underlying these KP steps are presently unknown but are thought to be TCR-proximal. This is consistent with the observation that the discrimination power depends on coreceptors that act proximal but is similar for different T cell responses (Fig. 4D-F). These share the same TCR-proximal signalling mechanism but are regulated by different downstream signalling pathways. Recent studies have suggested that slow LAT phosphorylation by ZAP70 is implicated in discrimination (44, 45). Although altering the rate of LAT phosphorylation by ZAP70 clearly impacted TCR sensitivity to antigen dose (45), our analysis suggests that this did not alter TCR discriminatory power ($\alpha = 1.1$, Table S1 ID 7 and 9). Thus LAT phosphorylation may be more important for antigen sensitivity than discrimination.

A number of different methods have been employed to analyse discrimination by T cells (23, 25, 29, 32, 34). Here, we have introduced the discrimination power (α) because it can robustly quantify discrimination from experimental data from different studies and it is independent of antigen sensitivity. Previously, the term specificity has been used to refer to this capacity. However, specificity is also used to mean the opposite of promiscuity (i.e. the ability of T cells to respond to many different peptides) (78). To avoid ambiguity, we suggest that specificity and promiscuity are used to refer to the tolerance of peptide sequence diversity while discrimination is used to refer to the tolerance of changes in TCR/pMHC binding parameters.

Our finding that the TCR exhibits higher discrimination than other receptors, such as cytokine receptors and RTKs (Fig. 5F), is interesting as the latter receptors also exhibit a multi-step signal transduction process akin to KP. The preliminary observation that the BCR, like the TCR, may also exhibit enhanced discrimination, suggests that it may be a shared feature of ITAM-based signalling. Another distinct feature of TCRs and BCRs is that they recognise surface anchored ligands whereas other receptors recognise ligands directly from solution (79). These features are also shared by synthetic CARs that, with available data, appear to exhibit baseline discrimination but they appear to have major defects in antigen recognition and signalling (80, 81). These observations may provide clues to the molecular mechanisms underlying discrimination.

The more modest discrimination power that we report for the TCR highlights the important role for established T-cell extrinsic mechanisms of tolerance, such as dependence on the APC (e.g. costimulatory and inhibitory receptor ligands) and other cells (e.g. T_{regs}). Moreover, it highlights that the concentration of lower-affinity antigens can have important roles in regulating T cell responses in pathology and in normal immune surveillance (15, 16).

Materials & Methods

We provide supplementary tables that contain information on each calculation of α for TCRs (Table S1) and non-TCR receptors (Table S2), and in addition, provide specific details on the source of data underlying each calculation (see Supplementary Information).

The broad method was to obtain a measure of ligand potency from each study. If provided by the study, this was often an EC_{50}, which is the concentration of ligand eliciting 50% of the maximum response. If not explicitly provided, we estimated ligand potency as P_X, which was defined by the concentration of ligand that produced X response. To do this, we drew a horizontal line at X on a provided dose-response graph and estimated the ligand concentration where the data intercepted the horizontal line. The disadvantage with this method is that ligand potency was estimated based on the single representative graph provided in the

study.

Each study often contained or cited a study that contained estimates of K_D or k_{off} for the specific TCR/pMHC interactions used in the study. We only included studies where monomeric SPR binding data was available to avoid multimeric binding parameters (e.g. when using tetramers). However, when analysing discrimination by other non-TCR receptors, we included binding data from various methods (e.g. SPR, radio labelled ligands) provided they were monomeric measurements. The use of SPR is important for weak interactions, such as TCR/pMHC, but various methods are available for higher affinity interactions.

The plot of potency over K_D or k_{off} was fit using linear regression on log-transformed axes. We reported the slope of the fit (i.e. the discrimination power, α), the goodness-of-fit measure (R^2), and the P-value for the null hypothesis that the slope is zero (i.e. $\alpha = 0$). We defined significance using the threshold of p=0.05.

A subset of the data relied on engineered high affinity TCR/pMHC interactions. It has been observed that increasing the affinity beyond a threshold does not improve ligand potency (11, 82). To avoid underestimating the discrimination power, we found that globally removing data where $K_D < 1$ μM avoided entering this saturation regime (with a single exception, see ID 58-61 in Supplementary Information and Fig S3-4). Similarly, to avoid over-estimating α, we did not include data where the potency was extrapolated (i.e. when EC_{50} values were larger than the highest ligand concentration tested). Some studies provided multiple measures of T cell responses and in this case, we produced potency plots for each response and hence were able to obtain multiple estimates of α.

We only included discrimination powers in final comparisons (Fig. 4, Fig. 5F) that were statistically significant ($p < 0.05$) with the exception of the original and revised mouse TCR data (Fig. 4A) because only few data were available. We found more studies that performed functional experiments on the original mouse TCRs compared to those that measured binding and therefore, to avoid introducing a potential bias in the analysis, we included only a single calculated α for each independent SPR measurement. In the case of the original mouse TCR data, we included 4 calculations of α (Table S1, ID 1, 2, 11, 14) and in the case of the revised mouse TCR data, we included 6 calculations of α (Table S1, ID 5, 13, 15, 17, 18, 19). However, we explicit include all α values we calculated in Table S1 where it is clear that including them would not impact any conclusions. We also note that discrimination powers obtained using artificial conditions, when antigen was presented on plates as recombinant protein or when presented on APCs but co-receptor was blocked, were *not* included in aggregated analyses (Fig. 4A-D, Fig. 5F).

All statistical analyses of α were performed using parametric 1-way ANOVA and/or multiple t-tests (with the stated correction for multiple comparisons) on log-transformed data.

Acknowledgements

We thank Ignacio Moraga Gonzalez, David K. Cole, David R. Greaves, Johannes Pettmann, Enas Abu Shah for helpful discussions.

Author contribution

AH, PAvdM, and OD conceived the study. AH performed the literature search with input from PAvdM and OD. AH performed all data analysis. AH, PAvdM, and OD interpreted data. AH and DBW performed mathematical modelling. AH drafted the manuscript that was subsequently revised by all authors.

Funding

The work was funded by a Wellcome Trust Senior Fellowship in Basic Biomedical Sciences (207537/Z/17/Z to OD), a National Science Foundation Division of Mathematical Sciences USA (NSF-DMS 1902854 for DBW), an Edward Penley Abraham Trust Studentship (to AH).

Conflicts of interest

The authors declare that they do not have any conflicts of interest.

References

1. Feinerman O, Germain RN, Altan-Bonnet G (2008) Quantitative challenges in understanding ligand discrimination by alphabeta T cells. *Molecular immunology* 45:619–31.

2. van der Merwe PA, Dushek O (2011) Mechanisms for T cell receptor triggering. *Nature Reviews Immunology* 11:47–55.

3. Chakraborty AK, Weiss A (2014) Insights into the initiation of TCR signaling. *Nature Immunology* 15:798–807.

4. Hogquist KA, Jameson SC, Bevan MJ (1995) Strong agonist ligands for the T cell receptor do not mediate positive selection of functional CD8+ T cells. *Immunity* 3:79–86.

5. Alam SM, et al. (1996) T cell-receptor affinity and thymocyte positive selection. *Nature* 381:616–620.

6. Alam S, et al. (1999) Qualitative and Quantitative Differences in T Cell Receptor Binding of Agonist and Antagonist Ligands. *Immunity* 10:227–237.

7. Kersh GJ, Allen PM (1996) Structural basis for T cell recognition of altered peptide ligands: a single T cell receptor can productively recognize a large continuum of related ligands. *J Exp Med* 184:1259–1268.

8. Kersh GJ, Kersh EN, Fremont DH, Allen PM (1998) High- and low-potency ligands with similar affinities for the TCR: the importance of kinetics in TCR signaling. *Immunity* 9:817–26.

9. Lyons DS, et al. (1996) A TCR binds to antagonist ligands with lower affinities and faster dissociation rates than to agonists. *Immunity* 5:53–61.

10. Aleksic M, et al. (2010) Dependence of T cell antigen recognition on T cell receptor-peptide MHC confinement time. *Immunity* 32:163–74.

11. Lever M, et al. (2016) A minimal signalling architecture explains the T cell response to a 1,000,000-fold variation in antigen affinity and dose. *Proc Natl Acad Sci USA* pp E6630–E6638.

12. Kersh GJ, Kersh EN, Fremont DH, Allen PM (1998) High- and low-potency ligands with similar affinities for the TCR: The importance of kinetic in TCR signaling. *Immunity* 9:817–826.

13. Yin Y, Li Y, Mariuzza RA (2012) Structural basis for self-recognition by autoimmune T-cell receptors. *Immunological Reviews* 250:32–48.

14. Bridgeman JS, Sewell AK, Miles JJ, Price DA, Cole DK (2012) Structural and biophysical determinants of $\alpha\beta$ T-cell antigen recognition. *Immunology* 135:9–18.

15. Korem Kohanim Y, Tendler A, Mayo A, Friedman N, Alon U (2020) Endocrine Autoimmune Disease as a Fragility of Immune Surveillance against Hypersecreting Mutants. *Immunity* 52:872–884.e5.

16. Wang J, et al. (2020) HLA-DR15 Molecules Jointly Shape an Autoreactive T Cell Repertoire in Multiple Sclerosis. *Cell* 2.

17. Lever M, Maini PK, van der Merwe PA, Dushek O (2014) Phenotypic models of T cell activation. *Nature Reviews Immunology* 14:619–629.

18. McKeithan TW (1995) Kinetic proofreading in T-cell receptor signal transduction. *Proceedings of the National Academy of Sciences of the United States of America* 92:5042–6.

19. Rabinowitz JD, Beeson C, Lyons DS, Davis MM, McConnell HM (1996) Kinetic discrimination in T-cell activation. *Proceedings of the National Academy of Sciences of the United States of America* 93:1401–5.

20. Huang J, et al. (2013) A Single Peptide-Major Histocompatibility Complex Ligand Triggers Digital Cytokine Secretion in CD4+ T Cells. *Immunity* pp 1–12.

21. Siller-Farfán JA, Dushek O (2018) Molecular mechanisms of T cell sensitivity to antigen. *Immunological Reviews* 285:194–205.

22. Chan C, George aJ, Stark J (2001) Cooperative enhancement of specificity in a lattice of T cell receptors. *Proceedings of the National Academy of Sciences of the United States of America* 98:5758–63.

23. Chan C, George AJ, Stark J (2003) T cell sensitivity and specificity - Kinetic proofreading revisited. *Discrete and Continuous Dynamical Systems - Series B* 3:343–360.

24. Chan C, Stark J, George AJT (2004) Feedback control of T-cell receptor activation. *Proceedings. Biological sciences / The Royal Society* 271:931–9.

25. Altan-Bonnet G, Germain RN (2005) Modeling T cell antigen discrimination based on feedback control of digital ERK responses. *PLoS biology* 3:e356.

26. Schamel WWa, Risueño RM, Minguet S, Ortíz AR, Alarcón B (2006) A conformation- and avidity-based proofreading mechanism for the TCR-CD3 complex. *Trends in immunology* 27:176–82.

27. Burroughs NJ, Lazic Z, van der Merwe PA (2006) Ligand detection and discrimination by spatial relocalization: A kinase-phosphatase segregation model of TCR activation. *Biophysical journal* 91:1619–29.

28. Dushek O, Das R, Coombs D (2009) A role for rebinding in rapid and reliable T cell responses to antigen. *PLoS computational biology* 5:e1000578.

29. Francois P, Voisinne G, Siggia ED, Altan-Bonnet G, Vergassola M (2013) Phenotypic model for early T-cell activation displaying sensitivity, specificity, and antagonism. *Proceedings of the National Academy of Sciences*.

30. Lalanne JB, François P (2013) Principles of Adaptive Sorting Revealed by In Silico Evolution. *Physical Review Letters* 110:218102.

31. Klotzsch E, Schütz G (2013) Improved Ligand Discrimination by Force-Induced Unbinding of the T Cell Receptor from Peptide-MHC. *Biophysical Journal* 104:1670–1675.

32. Dushek O, van der Merwe PA (2014) An induced rebinding model of antigen discrimination. *Trends in Immunology* 35:153–158.

33. Fernandes RA, et al. (2019) A cell topography-based mechanism for ligand discrimination by the T cell receptor. *Proceedings of the National Academy of Sciences of the United States of America* 116:14002–14010.

34. Ganti RS, et al. (2020) How the T cell signaling network processes information to discriminate between self and agonist ligands. *Proceedings of the National Academy of Sciences* p 202008303.

35. Wooldridge L, et al. (2012) A single autoimmune T cell receptor recognizes more than a million different peptides. *Journal of Biological Chemistry* 287:1168–1177.

36. Birnbaum ME, et al. (2014) Deconstructing the peptide-MHC specificity of t cell recognition. *Cell* 157:1073–1087.

37. Rosette C, et al. (2001) The Impact of Duration versus Extent of TCR Occupancy on T Cell Activation. *Immunity* 15:59–70.

38. Stepanek O, et al. (2014) Coreceptor scanning by the T cell receptor provides a mechanism for T cell tolerance. *Cell* 159:333–345.

39. Liu B, et al. (2015) The cellular environment regulates in situ kinetics of T-cell receptor interaction with peptide major histocompatibility complex. *European Journal of Immunology* 45:2099–2110.

40. Daniels MA, et al. (2006) Thymic selection threshold defined by compartmentalization of Ras/MAPK signalling. *Nature* 444:724–729.

41. Hong J, et al. (2015) Force-Regulated In Situ TCR–Peptide-Bound MHC Class II Kinetics Determine Functions of CD4 + T Cells . *The Journal of Immunology* 195:3557–3564.

42. Wu L, Tuot D, Lyons D, Garcia K, Davis M (2002) Competing interests statement Two-step binding mechanism for T-cell receptor recognition of peptide–MHC. *Nature* 418:552–556.

43. Newell EW, et al. (2011) Structural Basis of Specificity and Cross-Reactivity in T Cell Receptors Specific for Cytochrome c –I-E k . *The Journal of Immunology* 186:5823–5832.

44. Lo Wl, et al. (2018) Lck promotes Zap70-dependent LAT phosphorylation by bridging Zap70 to LAT. *Nature Immunology* 19.

45. Lo WL, et al. (2019) Slow phosphorylation of a tyrosine residue in LAT optimizes T cell ligand discrimination. *Nature Immunology* 20:1481–1493.

46. Richard AC, et al. (2018) T cell cytolytic capacity is independent of initial stimulation strength. *Nature Immunology* 19.

47. Abu-Shah E, et al. (2020) Human CD8 + T Cells Exhibit a Shared Antigen Threshold for Different Effector Responses . *The Journal of Immunology* p ji2000525.

48. Ma CY, Marioni JC, Griffiths GM, Richard AC (2020) Stimulation strength controls the rate of initiation but not the molecular organization of tcr-induced signalling. *eLife* 9:1–57.

49. Holler PD, Kranz DM (2003) Quantitative analysis of the contribution of TCR/pepMHC affinity and CD8 to T cell activation. *Immunity* 18:255–64.

50. Li QJ, et al. (2004) CD4 enhances T cell sensitivity to antigen by coordinating Lck accumulation at the immunological synapse. *Nature immunology* 5:791–799.

51. Laugel B, et al. (2007) Different T cell receptor affinity thresholds and CD8 coreceptor dependence govern cytotoxic T lymphocyte activation and tetramer binding properties. *Journal of Biological Chemistry* 282:23799–23810.

52. Burrows SR, et al. (2010) Hard wiring of t cell receptor specificity for the major histocompatibility complex is underpinned by tcr adaptability. *Proceedings of the National Academy of Sciences* 107:10608–10613.

53. Dushek O, et al. (2011) Antigen potency and maximal efficacy reveal a mechanism of efficient T cell activation. *Science Signaling* 4:ra39.

54. Trendel N, et al. (2020) Perfect adaptation of CD8 + T cell responses to constant antigen input over a wide range of affinity is overcome by costimulation. *Science Signaling (in press)*.

55. Levin AM, et al. (2012) Exploiting a natural conformational switch to engineer an interleukin-2 'superkine'. *Nature* 484:529–533.

56. Moraga I, et al. (2015) Instructive roles for cytokine-receptor binding parameters in determining signaling and functional potency. *Science Signaling* 8:1–17.

57. Thomas C, et al. (2011) Structural linkage between ligand discrimination and receptor activation by type i interferons. *Cell* 146:621–632.

58. Mendoza JL, et al. (2017) The IFN-λ-IFN-λR1-IL-10Rβ Complex Reveals Structural Features Underlying Type III IFN Functional Plasticity. *Immunity* 46:379–392.

59. Martinez-Fabregas J, et al. (2019) Kinetics of cytokine receptor traffi 1 cking determine signaling and functional selectivity. *eLife* 8:1–32.

60. Ho CCM, et al. (2017) Decoupling the functional pleiotropy of stem cell factor by tuning c-kit signaling. *Cell* 168:1041–1052.

61. Reddy CC, Niyogi SK, Wells A, Wiley HS, Lauffenburger DA (1996) Engineering epidermal growth factor for enhanced mitogenic potency. *Nature biotechnology* 14:1696–1699.

62. Sykes DA, Dowling MR, Charlton SJ (2009) Exploring the mechanism of agonist efficacy: a relationship between efficacy and agonist dissociation rate at the muscarinic m3 receptor. *Molecular pharmacology* 76:543–551.

63. Guo D, Mulder-Krieger T, IJzerman AP, Heitman LH (2012) Functional efficacy of adenosine a2a receptor agonists is positively correlated to their receptor residence time. *British journal of pharmacology* 166:1846–1859.

64. Guyon A, et al. (2013) Baclofen and other GABAB receptor agents are allosteric modulators of the CXCL12 chemokine receptor CXCR4. *Journal of Neuroscience* 33:11643–11654.

65. Heise CE, et al. (2005) Pharmacological characterization of CXC chemokine receptor 3 ligands and a small molecule antagonist. *Journal of Pharmacology and Experimental Therapeutics* 313:1263–1271.

66. Chmielewski M, Hombach A, Heuser C, Adams GP, Abken H (2004) T cell activation by antibody-like immunoreceptors: increase in affinity of the single-chain fragment domain above threshold does not increase t cell activation against antigen-positive target cells but decreases selectivity. *The Journal of Immunology* 173:7647–7653.

67. Liu X, et al. (2015) Affinity-tuned erbb2 or egfr chimeric antigen receptor t cells exhibit an increased therapeutic index against tumors in mice. *Cancer research* 75:3596–3607.

68. Taylor MJ, Husain K, Gartner ZJ, Mayor S, Vale RD (2017) A DNA-based T cell receptor reveals a role for receptor clustering in ligand discrimination. *Cell* 169:108–119.

69. Batista FD, Neuberger MS (1998) Affinity dependence of the b cell response to antigen: a threshold, a ceiling, and the importance of off-rate. *Immunity* 8:751–759.

70. Pettmann J, et al. (2020) T cells exhibit unexpectedly low discriminatory power and can respond to ultra-low affinity peptide-MHC ligands. *bioRxiv (preprint)*.

71. Adams JJ, et al. (2011) T cell receptor signaling is limited by docking geometry to peptide-major histocompatibility complex. *Immunity* 35:681–693.

72. Liu B, Chen W, Evavold BD, Zhu C (2014) Accumulation of Dynamic Catch Bonds between TCR and Agonist Peptide-MHC Triggers T Cell Signaling. *Cell* 157:357–68.

73. Sibener LV, et al. (2018) Isolation of a Structural Mechanism for Uncoupling T Cell Receptor Signaling from Peptide-MHC Binding. *Cell* 174:672–687.e27.

74. Huang J, et al. (2010) The kinetics of two-dimensional TCR and pMHC interactions determine T-cell responsiveness. *Nature* 464:932–6.

75. Cole DK, et al. (2016) Hotspot autoimmune T cell receptor binding underlies pathogen and insulin peptide cross-reactivity. *Journal of Clinical Investigation* 126:2191–2204.

76. Tischer DK, Weiner OD (2019) Light-based tuning of ligand half-life supports kinetic proofreading model of T cell signaling. *eLife* 8:1–25.

77. Huse M, et al. (2007) Spatial and temporal dynamics of T cell receptor signaling with a photoactivatable agonist. *Immunity* 27:76–88.

78. Sewell AK (2012) Why must T cells be cross-reactive? *Nature Reviews Immunology* 12:669–677.

79. Dushek O, Goyette J, van der Merwe PA (2012) Non-catalytic tyrosine-phosphorylated receptors. *Immunological Reviews* 250:258–276.

80. Harris DT, et al. (2017) Comparison of T Cell Activities Mediated by Human TCRs and CARs That Use the Same Recognition Domains. *The Journal of Immunology* p ji1700236.

81. Gudipati V, et al. (2019) Inefficient ZAP70-Signaling Blunts Antigen Detection by CAR-T-Cells. *bioRxiv* p 720417.

82. Irving M, et al. (2012) Interplay between T cell receptor binding kinetics and the level of cognate peptide presented by major histocompatibility complexes governs CD8+ T cell responsiveness. *The Journal of biological chemistry* 287:23068–78.

83. Kersh EN, Shaw aS, Allen PM (1998) Fidelity of T cell activation through multistep T cell receptor zeta phosphorylation. *Science (New York, N.Y.)* 281:572–5.

84. Persaud SP, Donermeyer DL, Weber KS, Kranz DM, Allen PM (2010) High-affinity T cell receptor differentiates cognate peptide-MHC and altered peptide ligands with distinct kinetics and thermodynamics. *Molecular Immunology* 47:1793–1801.

85. Krogsgaard M, Prado N, Adams E, He Xl (2003) Evidence that structural rearrangements and/or flexibility during TCR binding can contribute to T cell activation. *Molecular cell* 12:1367–1378.

86. Tian S, Maile R, Collins E, Frelinger J (2007) CD8+ T cell activation is governed by TCR-peptide/MHC affinity, not dissociation rate. *The Journal of Immunology* 179:2952.

87. Govern CC, Paczosa MK, Chakraborty AK, Huseby ES (2010) Fast on-rates allow short dwell time ligands to activate T cells. *Proceedings of the National Academy of Sciences* 107:8724–9.

88. Chervin AS, et al. (2009) The impact of TCR-binding properties and antigen presentation format on T cell responsiveness. *Journal of immunology* 183:1166–78.

89. Bowerman NA, et al. (2009) Engineering the binding properties of the t cell receptor: peptide: Mhc ternary complex that governs t cell activity. *Molecular immunology* 46:3000–3008.

90. Jones LL, Colf LA, Stone JD, Garcia KC, Kranz DM (2008) Distinct cdr3 conformations in tcrs determine the level of cross-reactivity for diverse antigens, but not the docking orientation. *The Journal of Immunology* 181:6255–6264.

91. Adams JJ, et al. (2016) Structural interplay between germline interactions and adaptive recognition determines the bandwidth of tcr-peptide-mhc cross-reactivity. *Nature immunology* 17:87–94.

92. McMahan RH, et al. (2006) Relating TCR-peptide-MHC affinity to immunogenicity for the design of tumor vaccines. *Journal of Clinical Investigation* 116:2543–2551.

93. Schmid Da, et al. (2010) Evidence for a TCR affinity threshold delimiting maximal CD8 T cell function. *Journal of immunology (Baltimore, Md. : 1950)* 184:4936–4946.

94. Thomas S, et al. (2011) Human t cells expressing affinity-matured tcr display accelerated responses but fail to recognize low density of mhc-peptide antigen. *Blood, The Journal of the American Society of Hematology* 118:319–329.

95. Thomas S, et al. (2011) Human T cells expressing affinity-matured TCR display accelerated responses but fail to recognize low density of MHC-peptide antigen. *Blood* 118:319–29.

96. Zhong S, et al. (2013) T-cell receptor affinity and avidity defines antitumor response and autoimmunity in T-cell immunotherapy. *Proceedings of the National Academy of Sciences*.

97. Bianchi V, et al. (2016) A Molecular Switch Abrogates Glycoprotein 100 (gp100) T-cell Receptor (TCR) Targeting of a Human Melanoma Antigen. *Journal of Biological Chemistry* 291:8951–8959.

98. Andersen PS, Geisler C, Buus S, Mariuzza Ra, Karjalainen K (2001) Role of the T cell receptor ligand affinity in T cell activation by bacterial superantigens. *The Journal of biological chemistry* 276:33452–7.

99. Andersen PS, Menné C, Mariuzza Ra, Geisler C, Karjalainen K (2001) A response calculus for immobilized T cell receptor ligands. *The Journal of biological chemistry* 276:49125–32.

100. Tan MP, et al. (2015) T cell receptor binding affinity governs the functional profile of cancer-specific CD8+ T cells. *Clinical & Experimental Immunology* 180:255–270.

101. Chan KF, et al. (2018) Divergent T-cell receptor recognition modes of a HLA-I restricted extended tumour-associated peptide. *Nature Communications* 9.

102. Broughton SE, et al. (2012) Biased t cell receptor usage directed against human leukocyte antigen dq8-restricted gliadin peptides is associated with celiac disease. *Immunity* 37:611–621.

103. Benati D, et al. (2016) Public t cell receptors confer high-avidity cd4 responses to hiv controllers. *The Journal of clinical investigation* 126:2093–2108.

104. Ekeruche-Makinde J, et al. (2012) T-cell receptor-optimized peptide skewing of the t-cell repertoire can enhance antigen targeting. *Journal of Biological Chemistry* 287:37269–37281.

105. Madura F, et al. (2019) Tcr-induced alteration of primary mhc peptide anchor residue. *European journal of immunology* 49:1052–1066.

106. Chmielewski M, Hombach A, Heuser C, Adams GP, Abken H (2004) T Cell Activation by Antibody-Like Immunoreceptors: Increase in Affinity of the Single-Chain Fragment Domain above Threshold Does Not Increase T Cell Activation against Antigen-Positive Target Cells but Decreases Selectivity. *The Journal of Immunology* 173:7647–7653.

107. Zehn D, Lee SY, Bevan MJ (2009) Complete but curtailed T cell response to very low affinity antigen. *Nature* 458:211–214.

108. Birnbaum ME, Dong S, Garcia KC (2012) Diversity-oriented approaches for interrogating T-cell receptor repertoire, ligand recognition, and function. *Immunological reviews* 250:82–101.

109. Govern CC, Paczosa MK, Chakraborty AK, Huseby ES (2010) Fast on-rates allow short dwell time ligands to activate t cells. *Proceedings of the National Academy of Sciences* 107:8724–8729.

110. Chervin AS, et al. (2009) The impact of tcr-binding properties and antigen presentation format on t cell responsiveness. *The Journal of Immunology* 183:1166–1178.

111. McMahan RH, et al. (2006) Relating tcr-peptide-mhc affinity to immunogenicity for the design of tumor vaccines. *The Journal of clinical investigation* 116:2543–2551.

112. Schmid DA, et al. (2010) Evidence for a tcr affinity threshold delimiting maximal cd8 t cell function. *The Journal of Immunology* 184:4936–4946.

Supplementary Information
The discriminatory power of the T cell receptor

Anna Huhn[1], Daniel B. Wilson[1,2], P. Anton van der Merwe[1], Omer Dushek[1¶]

[1]Sir William Dunn School of Pathology, University of Oxford, OX1 3RE, Oxford, UK
[2]Boston University, Department of Mathematics and Statistics, Boston, MA 02215
[¶]Corresponding author (omer.dushek@path.ox.ac.uk)

Supplementary Tables

Table S1: Overview of discrimination powers for TCRs (see also Excel Spreadsheet). Each row is associated with an experimental ID that is linked to detailed information on how the data was extracted (see Supplementary Information text) and the potency plots (Fig. S1,S2,S3,S4).

	Receptor and Ligand			Potency Assay			References		Fitting Result					
ID	TCR	Peptide	Species	Assay	**Coreceptor**	Output	Ref SPR measurement	Ref Potency measurement	Power	Std Error	R squared	P-value	signf	n
1	OT-I	OVA (257-264)	Mouse	Cellular	Yes	Lysis	Alam 1996 (5)	Hogquist 1995 (4)	12.	Perfect line	1.0		ns	2
2	OT-I	OVA (257-264)	Mouse	Cellular	Yes	Lysis	Alam 1999 (6)	Hogquist 1995 (4)	10.	2.4	0.95	0.14	ns	3
3	OT-I	OVA (257-264)	Mouse	Plate	Yes	CD69	Rosette 2001 (37)	Rosette 2001 (37)	18.13	Perfect line	1.0		ns	2
4	OT-I	OVA (257-264)	Mouse	Cellular	Yes	pERK	Alam 1999 (6)	Altan-Bonnet 2005 (25)	>5.1	1.9	0.88	0.23	ns	1(3)
5	OT-I	OVA (257-264)	Mouse	Cellular	Yes	CD69	Stepanek 2014 (38)	Daniels 2006 (40)	2.1	0.33	0.93	0.0084	sig	5
6	OT-I	OVA (257-264)	Mouse	Cellular	Yes	IFNγ	Stepanek 2014 (38)	Zehn 2009 (40)	2.0	Perfect line	1		ns	2
7	OT-I	OVA (257-264)	Mouse	Cellular	Yes	CD69	Stepanek 2014 (38)	Lo 2019 (45)	1.1	0.27	0.89	0.055	ns	4
8	OT-I	OVA (257-264)	Mouse	Cellular	No	CD69	Stepanek 2014 (38)	Lo 2019 (45)	0.37	0.12	0.84	0.084	ns	4
9	OT-I	OVA (257-264)	Mouse	Cellular	Yes	CD69	Stepanek 2014 (38)	Lo 2019 (45) (G131D)	1.1	0.12	0.98	0.010	sig	4
10	OT-I	OVA (257-264)	Mouse	Cellular	No	CD69	Stepanek 2014 (38)	Lo 2019 (45) (G131D)	1.4	0.19	0.96	0.020	sig	4
11	3.L2	Hb (64-76)	Mouse	Cellular	Yes	Lysis	Kersh 1998 (83) (k_{off})	Kersh 1996 (7)	6.8	0.61	0.98	0.008	sig	4
12	3.L2	Hb (64-76)	Mouse	Cellular	Yes	Lysis	Persaud 2010 (84)	Persaud 2010 (84)	0.37	0.37	0.25	0.39	ns	5
13	3.L2	Hb (64-76)	Mouse	Cellular	Yes	Lysis	Hong 2015 (41)	Kersh 1996 (7)	3.2	0.37	0.97	0.013	sig	4
14	2B4	MCC (88-103)	Mouse	Cellular	Yes	IL-2	Lyons 1996 (9)	Lyons 1996 (9)	6.7	Perfect line	1		ns	2
15	2B4	MCC (88-103)	Mouse	Cellular	Yes	IL-2	Krogsgaard 2003 (85)	Lyons 1996 (9)	2.19	Perfect line	1		ns	2
16	2B4	MCC (88-103)	Mouse	Plate	Yes	IL-2	Krogsgaard 2003 (85)	Krogsgaard 2003 (85)	1.2	0.41	0.65	0.030	sig	7
17	2B4	MCC (88-103)	Mouse	Cellular	Yes	IL-2	Wu 2002 (42)	Lyons 1996 (9)	2.8	Perfect line	1		ns	
18	2B4	MCC (88-103)	Mouse	Cellular	Yes	IL-2	Newell 2011 (43)	Newell 2011 (43)	2.3	0.30	0.97	0.017	sig	4
19	2B4	MCC (88-103)	Mouse	Cellular	Yes	IL-2	Birnbaum 2014 (36)	Birnbaum 2014 (36)	0.95	0.24	0.84	0.029	sig	5
20	5cc7	MCC (88-103)	Mouse	Cellular	Yes	IL-2	Birnbaum 2014 (36)	Birnbaum 2014 (36)	0.74	0.99	0.16	0.51	ns	5
21	P14	gp33 (33–41)	Mouse	Plate	Yes	IFNγ	Tian 2007 (86)	Tian 2007 (86)	1.3	0.29	0.67	0.0011	sig	12
22	P14	gp33 (33–41)	Mouse	Cellular	Yes	Lysis	Tian 2007 (86)	Tian 2007 (86)	2.1	0.87	0.49	0.054	ns	12
23	B3K506	3K	Mouse	Cellular	Yes	Proliferation	Govern 2010 (87)	Govern 2010 (87)	2.9	0.32	0.92	<0.0001	sig	9
24	B3K506	3K	Mouse	Cellular	Yes	TNFα	Govern 2010 (87)	Govern 2010 (87)	2.4	0.22	0.95	<0.0001	sig	8
25	B3K508	3K	Mouse	Cellular	Yes	Proliferation	Govern 2010 (87)	Govern 2010 (87)	2.9	0.17	1.0	0.036	sig	3
26	B3K508	3K	Mouse	Cellular	Yes	TNFα	Govern 2010 (87)	Govern 2010 (87)	2.5	0.14	1.0	0.037	sig	3
27	2C	SIYR	Mouse	Plate	No	IL-2	Chervin 2009 (88)	Chervin 2009 (88)	0.12	0.19	0.17	0.59	ns	4
28	2C	SIYR	Mouse	Cellular	No	IL-2	Chervin 2009 (88)	Chervin 2009 (88)	Too few points				ns	0
29	2C	SIYR	Mouse	Cellular	Yes	IL-2	Chervin 2009 (88)	Chervin 2009 (88)	0.66	1.7	0.069	0.74	ns	4
30	2C	QL9	Mouse	Cellular	Yes	IL-2	Bowerman 2009 (89)	Bowerman 2009 (89)	2.7	1.3	0.82	0.28	ns	2
31	2C	QL9 and SIYR	Mouse	Cellular	Yes	IL-2	Jones 2008 (90)	Jones 2008 (90)	4.7	1.4	0.92	0.18	ns	3
32	2C	QL9 and SIYR	Mouse	Cellular	No	IL-2	Jones 2008 (90)	Jones 2008 (90)	6.5	Perfect line	1		ns	2
33	42F3	QL9	Mouse	Cellular	Yes	IL-2	Adams 2016 (91)	Adams 2016 (91)	0.15	0.65	0.010	0.83	ns	8
34	AH1 specific	AH1 (gp70 423–431)	Mouse	Cellular	Yes	IFNγ	McMahan 2006 (92)	McMahan 2006 (92)	5.1	1.2	0.79	0.0072	sig	7
35	1G4	NY-ESO-1 (157-165)	Human	Cellular	Yes	Lysis	Irving 2012 (82)	Irving 2012 (82)	0.67	0.043	0.99	0.0041	sig	4
36	1G4	NY-ESO-1 (157-165)	Human	Cellular	Yes	Lysis	Schmid 2010 (93)	Schmid 2010 (93)	0.69	0.20	0.75	0.026	sig	7
37	1G4	NY-ESO-1 (157-165)	Human	Plate	Yes	IFNγ	Aleksic 2010 (10)	Aleksic 2010 (10)	0.60	0.12	0.63	0.0001	sig	17
38	1G4	NY-ESO-1 (157-165)	Human	Cellular	Yes	Lysis	Aleksic 2010 (10)	Aleksic 2010 (10)	1.6	0.21	0.89	0.0001	sig	9
39	1G4	NY-ESO-1 (157-165)	Human	Plate	Yes	IFNγ	Dushek 2011 (53)	Dushek 2011 (53)	0.55	0.17	0.63	0.019	sig	8
40	G10	gag p17	Human	Plate	Yes	IFNγ	Dushek 2011 (53)	Dushek 2011 (53)	0.95	0.16	0.79	0.0003	sig	9
41	1E6	INS	Human	Cellular	Yes	Lysis	Cole 2016 (75) (25°C)	Cole 2016 (75)	1.1	0.85	0.62	0.037	sig	7
42	1E6	INS	Human	Cellular	Yes	Lysis	Cole 2016 (75) (37°C)	Cole 2016 (75)	1.2	0.29	0.85	0.026	sig	5
43	A6	Tax (11-19)	Human	Cellular	Yes	CD107	Thomas 2011 (94)	Thomas 2011 (94)	2.0	0.38	0.97	0.12	ns	3
44	A6	Tax (11-19)	Human	Cellular	Yes	IFNγ	Thomas 2011 (95)	Thomas 2011 (95)	2.2	0.42	0.97	0.12	ns	2
45	gp209 TCR	gp100 (209–217)	Human	Cellular	Yes	IFNγ	Zhong 2013 (96)	Zhong 2013 (96)	1.3	0.54	0.74	0.14	ns	6
46	gp209 TCR	gp100 (209–217)	Human	Cellular	Yes	ppERK	Zhong 2013 (96)	Zhong 2013 (96)	1.2	0.84	0.41	0.25	ns	6
47	gp100 TCR	gp100 (280–288)	Human	Cellular	Yes	Lysis	Bianchi 2016 (97)	Bianchi 2016 (97)	2.3	0.73	0.71	0.036	sig	6
48	gp100 TCR	gp100 (280–288)	Human	Cellular	Yes	MIP-1β	Bianchi 2016 (97)	Bianchi 2016 (97)	3.6	0.54	0.92	0.0026	sig	6
49	14.3.d	SEC3	Human	Plate	No	NFAT	Andersen 2001 (98)	Andersen 2001 (98)	0.81	0.22	0.93	0.17	ns	3
50	14.3.d	F23.1	Human	Plate	No	NFAT	Andersen 2001 (99)	Andersen 2001 (98)	0.66	0.83	0.24	0.51	ns	4
51	TCR55	HIV Pol(448-456)	Human	Cellular	Yes	CD69	Sibener 2018 (73)	Sibener 2018 (73)	0.19	0.22	0.10	0.41	ns	9
52	ILA1	ILA	Human	Cellular	Yes	Degranulation	Laugel 2007 (51)	Laugel 2007 (51)	1.0	0.38	0.70	0.076	ns	4
53	ILA1	ILA	Human	Cellular	No	Degranulation	Laugel 2007 (51)	Laugel 2007 (51)	0.19	1.2	0.025	0.90	ns	4
54	ILA1	ILA	Human	Cellular	Yes	CD107a	Laugel 2007 (51)	Laugel 2007 (51)	2.2	0.30	0.96	0.018	sig	4
55	ILA1	ILA	Human	Cellular	No	CD107a	Laugel 2007 (51)	Laugel 2007 (51)	3.6	0.27	0.99	0.0055	sig	4
56	ILA1	ILA	Human	Cellular	Yes	IFNγ	Laugel 2007 (51)	Laugel 2007 (51)	2.2	0.39	0.94	0.03	sig	4
57	ILA1	ILA	Human	Cellular	No	IFNγ	Laugel 2007 (51)	Laugel 2007 (51)	3.2	0.41	0.97	0.015	sig	4
58	ILA1	ILA	Human	Cellular	Yes	MIP-1β	Tan 2015 (100)	Tan 2015 (100)	1.4	0.54	0.76	0.13	ns	5
59	ILA1	ILA	Human	Cellular	Yes	IFNγ	Tan 2015 (100)	Tan 2015 (100)	0.77	0.057	0.99	0.0054	sig	5
60	ILA1	ILA	Human	Cellular	Yes	TNFα	Tan 2015 (100)	Tan 2015 (100)	0.97	0.24	0.89	0.054	ns	5
61	ILA1	ILA	Human	Cellular	Yes	IL-2	Tan 2015 (100)	Tan 2015 (100)	1.1	0.084	0.99	0.0058	sig	5
62	KFJ	NY-ESO-1 (60-72)	Human	Cellular	Yes	TNFα	Chan 2018 (101)	Chan 2018 (101)	-0.59	0.99	0.15	0.61	ns	4
63	Gliadin TCR	Gliadin	Human	Cellular	Yes	Proliferation	Broughton 2012 (102)	Broughton 2012 (102)	0.83	0.027	1.0	0.021	sig	4
64	LC13	FLR	Human	Cellular	Yes	CD69	Burrows 2010 (52)	Burrows 2010 (52)	1.9	0.16	0.99	0.0075	sig	5
65	LC13	FLR	Human	Cellular	No	CD69	Burrows 2010 (52)	Burrows 2010 (52)	7.8	0.040	1	0.0033	sig	3
66	LC13	FLR	Human	Cellular	Yes	Lysis	Burrows 2010 (52)	Burrows 2010 (52)	4.1	2.1	0.80	0.30	ns	3
67	SB27	LPEP	Human	Cellular	Yes	Lysis	Burrows 2010 (52)	Burrows 2010 (52)	0.11	0.19	0.10	0.60	ns	5
68	gag TCR	Gag293 (HIV)	Human	Cellular	Yes	CD69	Benati 2016 (103)	Benati 2016 (103)	1.0	0.29	0.72	0.016	sig	7
69	MEL5	MART-1 (27-35)	Human	Cellular	Yes	MIP-1β	Ekeruche-Makinde 2012 (104)	Ekeruche-Makinde 2012 (104)	2.3	0.42	0.81	0.001	sig	6
70	MEL5	MART-1 (27-35)	Human	Cellular	Yes	MIP-1β	Madura 2019 (105)	Madura 2019 (105)	4.5	2.6	0.51	0.18	ns	6

Table S2: Overview of discrimination powers for non-TCR surface receptors (see also Excel Spreadsheet). Each row is associated with an experimental ID that is linked to detailed information on how the data was extracted (see Supplementary Information text) and the potency plots (Fig. S5,S6).

	Family	Receptor	Output	Ref Affinity measurement	Ref Potency measurement	Power	Std Error	R squared	P value	sig.	n
1	Cytokine	IL-2Rβ	pSTAT5 (NK cells)	Levin 2012 (55)	Levin 2012 (55)	0.55	0.031	0.99	0.0032	sig	4
2	Cytokine	IL-2Rβ	%pSTAT5 (T cells)	Levin 2012 (55)	Levin 2012 (55)	0.74	0.047	0.99	0.0039	sig	4
3	Cytokine	IL-13Rα1	pSTAT6	Moraga 2015 (56)	Moraga 2015 (56)	0.47	0.065	0.80	<0.0001	sig	9
4	Cytokine	IL-13Rα2	Proliferation	Moraga 2015 (56)	Moraga 2015 (56)	0.39	0.24	0.27	0.15	ns	9
5	Cytokine	IL-13Rα2	CD86	Moraga 2015 (56)	Moraga 2015 (56)	0.44	0.085	0.90	0.0139	sig	5
6	Cytokine	IL-13Rα1	CD205	Moraga 2015 (56)	Moraga 2015 (56)	0.42	0.048	0.96	0.0031	sig	9
7	Cytokine	IFNAR1/IFNAR2	antiviral	Thomas 2011 (57)	Thomas 2011 (57)	0.71	0.11	0.79	<0.0001	sig	13
8	Cytokine	IFNAR1/IFNAR2	antiproliferation	Thomas 2011 (57)	Thomas 2011 (57)	1.3	0.11	0.93	<0.0001	sig	13
9	Cytokine	IFN-γ R1-IL-10Rβ	pSTAT1	Mendoza 2017 (58)	Mendoza 2017 (58)	0.024	0.046	0.030	0.61	ns	11
10	Cytokine	IFN-γ R1-IL-10Rβ	antiviral	Mendoza 2017 (58)	Mendoza 2017 (58)	0.034	0.063	0.032	0.60	ns	11
11	Cytokine	IFN-γ R1-IL-10Rβ	antiproliferation	Mendoza 2017 (58)	Mendoza 2017 (58)	0.50	0.14	0.60	0.0054	sig	11
12	Cytokine	gp130 (and IL6Rα)	pSTAT1	Martinez-Fabregas 2019 (59)	Martinez-Fabregas 2019 (59)	0.54	0.24	0.84	0.26	ns	3
13	Cytokine	gp130 (and IL6Rα)	pSTAT3	Martinez-Fabregas 2019 (59)	Martinez-Fabregas 2019 (59)	0.52	0.32	0.57	0.24	ns	4
14	RTK	EGFR	growth rate	Reddy 1996 (61)	Reddy 1996 (61)	0.55	0.10	0.97	0.12	ns	3
15	RTK	c-Kit	pERK	Ho 2017 (60)	Ho 2017 (60)	0.83	0.14	0.95	0.028	sig	4
16	RTK	c-Kit	pAKT	Ho 2017 (60)	Ho 2017 (60)	0.88	0.14	0.96	0.023	sig	4
17	GPCR	A2A receptor	whole cell	Guo 2012 (63)	Guo 2012 (63)	0.29	0.20	0.22	0.19	ns	10
18	GPCR	A2A receptor	cAMP	Guo 2012 (63)	Guo 2012 (63)	0.71	0.29	0.42	0.041	sig	10
19	GPCR	M3 muscarinic receptor	Calcium	Sykes 2009 (62)	Sykes 2009 (62)	0.77	0.53	0.29	0.21	ns	7
20	GPCR	M3 muscarinic receptor	GTPγS Binding	Sykes 2009 (62)	Sykes 2009 (62)	0.55	0.18	0.65	0.029	sig	7
21	GPCR	CXCR4	Voltage	Guyon 2013 (64)	Guyon 2013 (64)	0.57	0.40	0.40	0.25	ns	5
22	GPCR	CXCR3	Calcium mobilization	Heise 2005 (65)	Heise 2005 (65)	0.73	0.033	1.0	0.029	sig	3
23	GPCR	CXCR3	GTPγS Binding	Heise 2005 (65)	Heise 2005 (65)	1.1	0.0039	1	0.0024	sig	3
24	GPCR	CXCR3	Migrated Cells	Heise 2005 (65)	Heise 2005 (65)	0.56	Perfect line	1		ns	2
25	CAR	C6.5 (scFc against ErbB2)	INFγ	Chmielewski 2004 (106)	Chmielewski 2004 (106)	0.52	0.028	0.99	0.0003	sig	5
26	CAR	ErB2	CD107	Liu 2015 (67)	Liu 2015 (67)	1.1	0.14	0.97	0.017	sig	4
27	CAR	ErB2	Proliferation	Liu 2015 (67)	Liu 2015 (67)	0.64	0.18	0.87	0.068	ns	4
28	CAR	DNA-CAR	pERK	Taylor 2017 (68)	Taylor 2017 (68)	1.2	0.17	0.96	0.019	sig	4
29	BCR	D1.3	IL2	Batista 1998 (69)	Batista 1998 (69)	1.4	0.18	0.94	0.0014	sig	
30	BCR	HyHEL10	IL2	Batista 1998 (69)	6 Batista 1998 (69)	1.3	0.12	0.98	0.0088	sig	4

Supplementary Figures

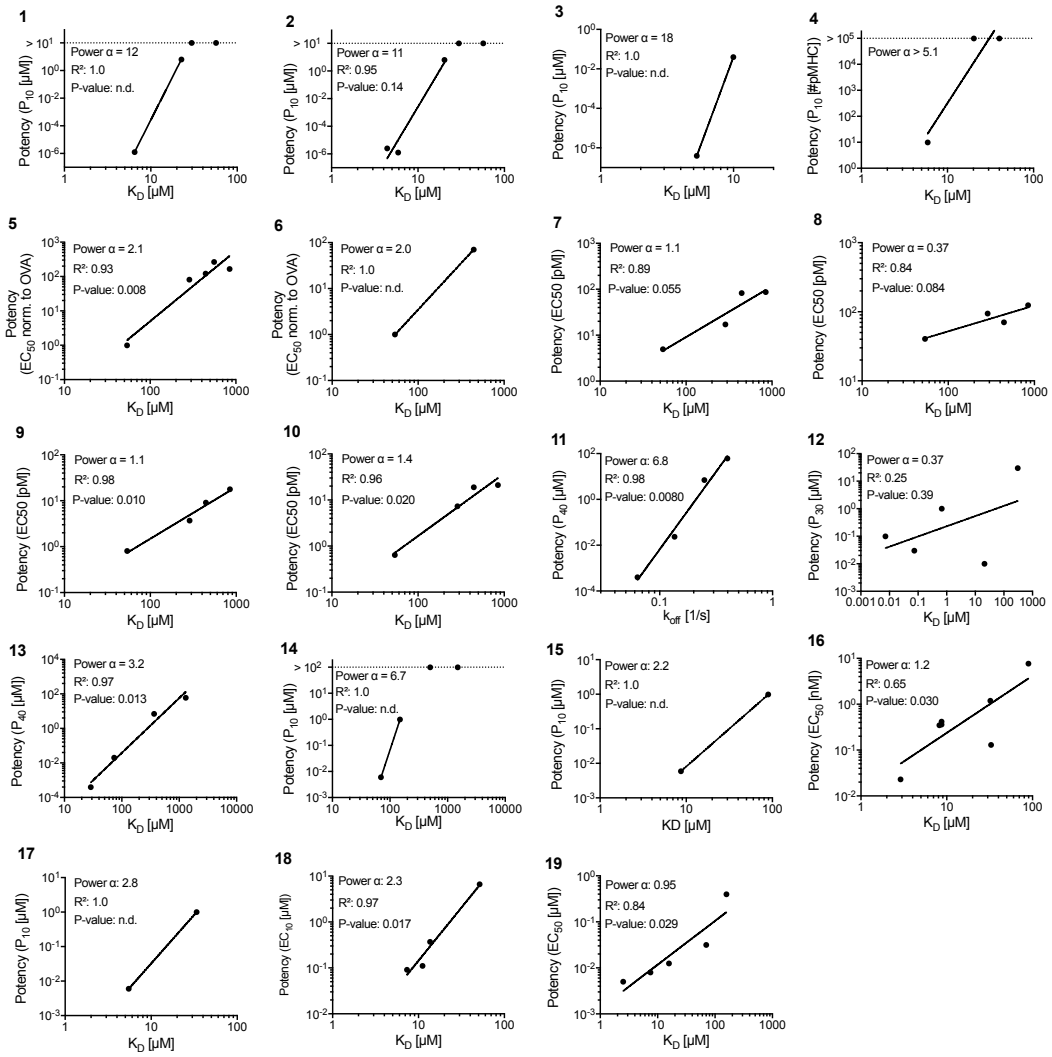

Figure S1: **Revised potency over K_D data for the original mouse TCRs** The fitted discrimination power (α), coefficient of determination (R^2), and p-value for the null hypothesis of a horizontal line (P-value) are indicated. Each panel is linked by an ID to a paragraph in the supplementary information.

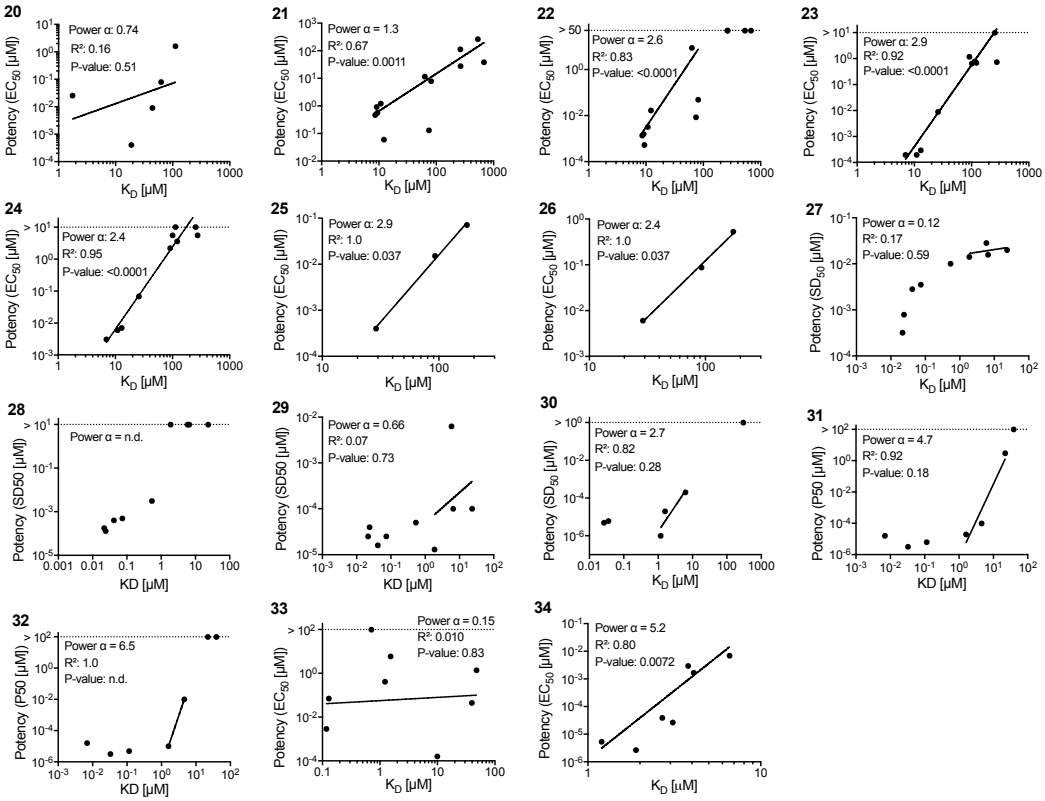

Figure S2: **Potency over K_D data for other mouse TCRs** The fitted discrimination power (α), coefficient of determination (R^2), and p-value for the null hypothesis of a horizontal line (P-value) are indicated. Each panel is linked by an ID to a paragraph in the supplementary information.

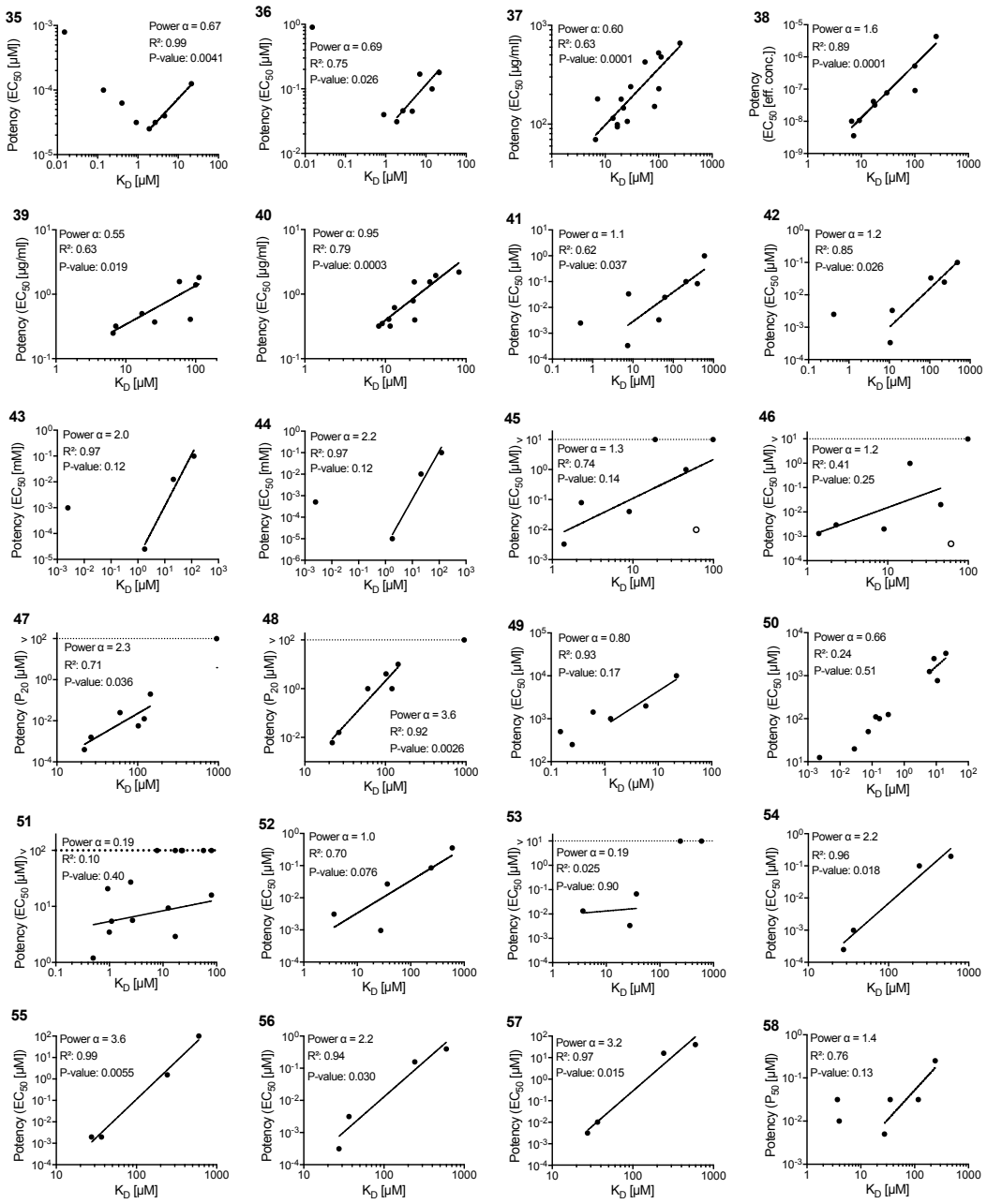

Figure S3: **Potency over K_D data for other human TCRs** The fitted discrimination power (α), coefficient of determination (R^2), and p-value for the null hypothesis of a horizontal line (P-value) are indicated. Each panel is linked by an ID to a paragraph in the supplementary information.

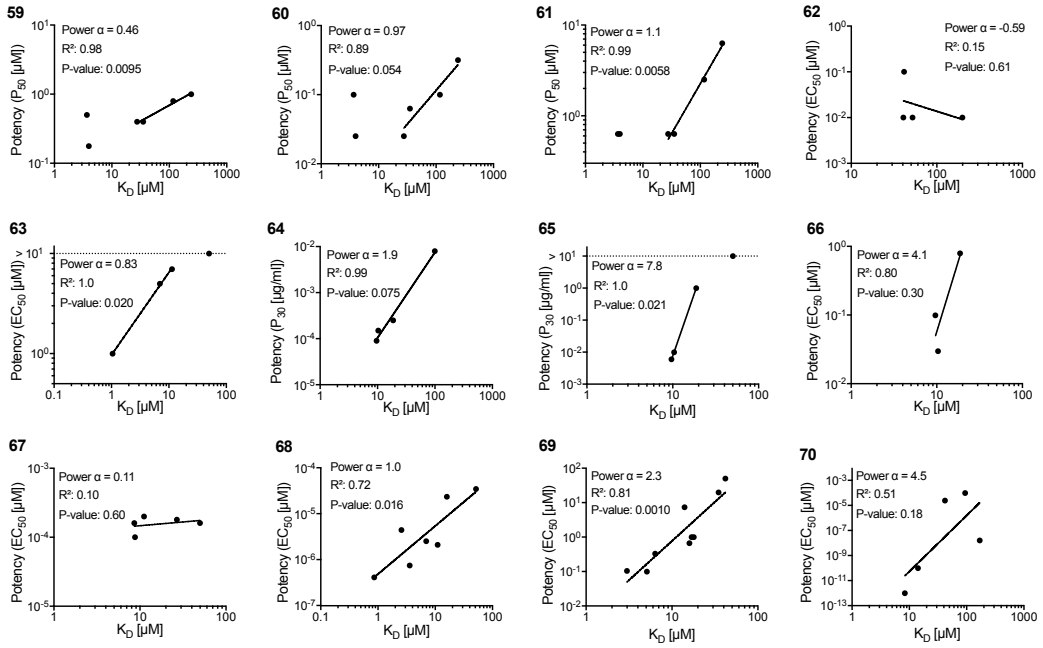

Figure S4: **Potency over K_D data for other human TCRs** The fitted discrimination power (α), coefficient of determination (R^2), and p-value for the null hypothesis of a horizontal line (P-value) are indicated. Each panel is linked by an ID to a paragraph in the supplementary information.

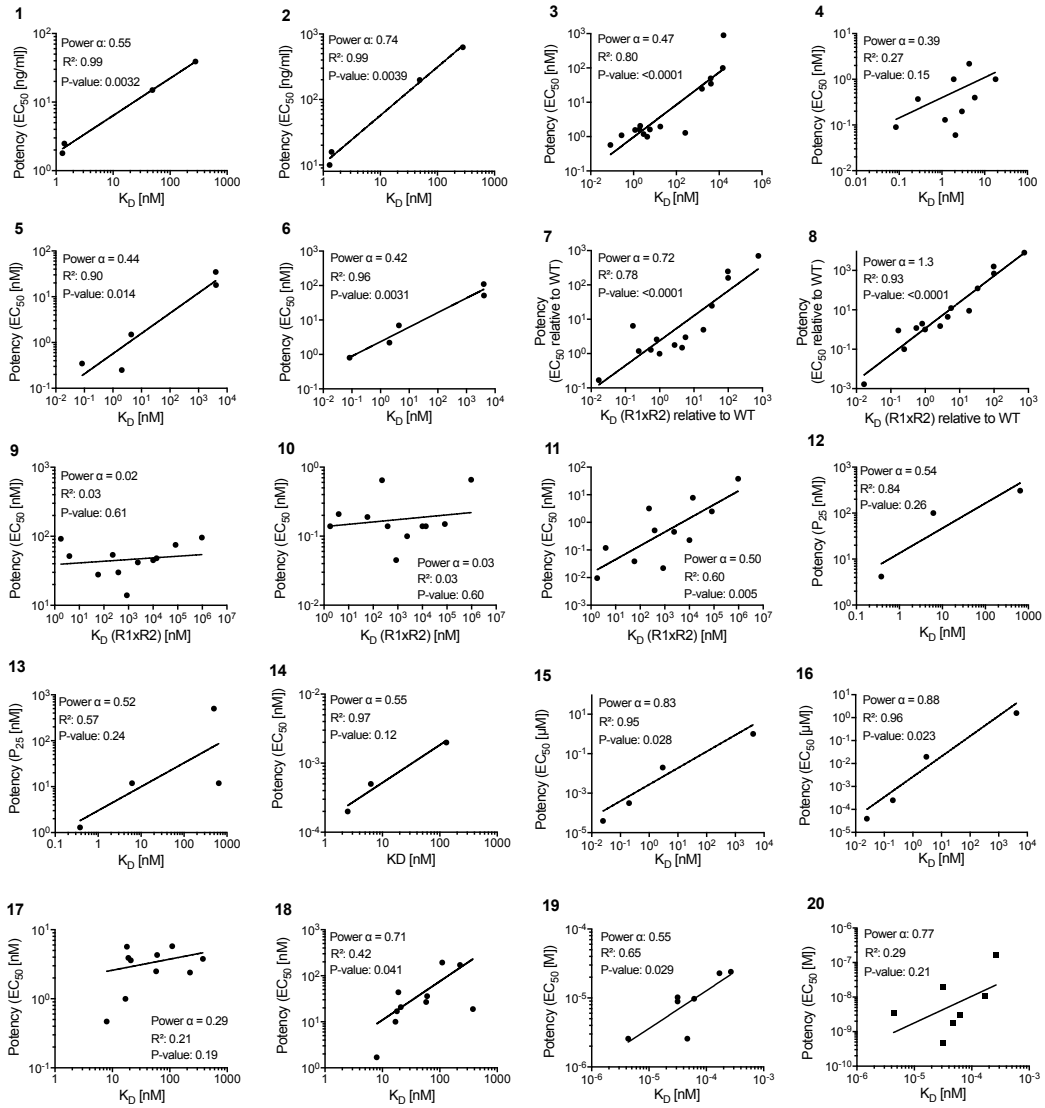

Figure S5: **Potency over K_D data for other (non-TCR) receptors** The fitted discrimination power (α), coefficient of determination (R^2), and p-value for the null hypothesis of a horizontal line (P-value) are indicated. Each panel is linked by an ID to a paragraph in the supplementary information.

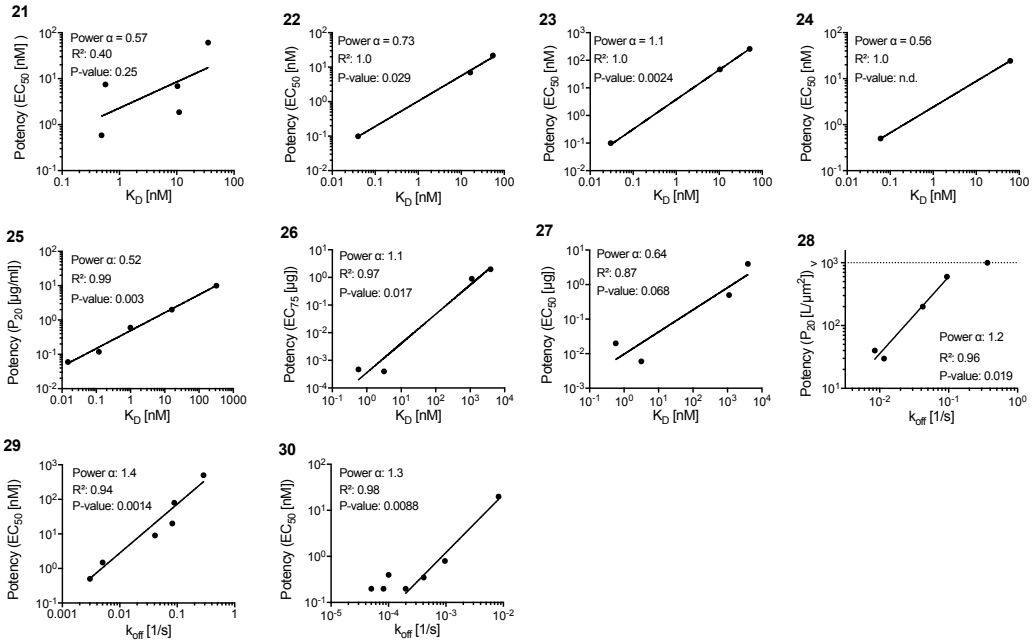

Figure S6: **Potency over K_D data for other (non-TCR) receptors** The fitted discrimination power (α), coefficient of determination (R^2), and p-value for the null hypothesis of a horizontal line (P-value) are indicated. Each panel is linked by an ID to a paragraph in the supplementary information.

Supplementary Text

Studies included in the analysis

We provide information on each potency plot we generated in the sections that follow, including the location of the potency and K_D data within each study. References to Figures and Tables are to those in the cited manuscript not to those in the present study. We provide the value of α produced and additional information, including R^2 and p-values are provided in Table S1 and S2.

Original mouse TCR data

OT-I

ID 1 (5) Experiments were performed with the murine transgenic TCR OT-I that binds to a peptide from ovalbumin (OVA) presented on H2Kb. Affinity was measured by SPR at 25°C. Affinity values were taken from Table 1 and Figure 3f. For the power analysis, we used K_D values estimated from the binding kinetics (kinetic K_D values). Potency measures for the OVA peptide and peptide variants were previously measured by Hogquist et al (4). OT-I T cell responses to OVA and single amino acid peptide variants (A2 and E1) were measured in a cell lysis assay. For the power analysis we extracted the potency of the peptides by reading the P_{10} (peptide concentration producing 10% specific lysis) from dose response curve in Figure 2. We excluded peptides that did not result in any response. We were able to include two data points with potency and affinity values for the power analysis producing $\alpha = 12$ (ID 1).

ID 2 (6) The OT-I TCR binding to the peptides derived from OVA were used with affinity and kinetics measured by SPR at 6, 25 and 37°C. Unusual biphasic binding was observed at 37°C for some peptides with two k_{on} and two k_{off} values reported based on a slow first and fast second step binding. Affinity values were provided in Table 1. To avoid picking the fast or slow phase parameters, we used the monophasic affinity data measured at 25°C for the power analysis. Potency data was taken from Hogquist et al (4). Three data points were included in the analysis producing $\alpha = 10$ (ID 2).

ID 3 (37) OT-I TCR affinity and functional activity was measured when binding its wild type ligand OVA or single amino acid variants (G4). Affinity values of TCR-pMHC interaction, measured by SPR at 25 and 37°C, were provided in Table 1. Similar to Alam et al (6), TCR binding to MHC loaded with OVA showed biphasic binding at 37°C. As before, we used the data measured at 25 °C for the power analysis. Functional data was generated with T cells isolated from OT-I transgenic mice. T cells were then stimulated with peptide-MHC complexes immobilised on plates. We read off potency data from dose response curves in Figure 1. Only two data points were available for calculating the discrimination power α producing $\alpha = 18$ (ID 3)

ID 4 (25) In this study, the OT-I T cell response when stimulated with OVA and was determined by phosphorylation of the kinase ERK in the MAPK pathway. Responses to OVA peptide as well as two

peptide variants were studied. Potency values were extracted as P_{10} from dose response curves in Figure 1C. Only the OVA peptide could activate T cells above background. Potency for unresponsive peptides was set to the highest concentration used in assay. Therefore, the discrimination power α calculated with these data points gives a lower bound on the actual value for α. Using the affinity data from Alam et al (6) produced $\alpha > 5.1$ (ID 4).

3.L2

ID 11 (83) This paper contains affinity and kinetic data for 3.L2 TCR which recognises murine haemoglobin (Hb 64-76) measured by SPR at 25 °C. We used k_{off} values for the power analysis as K_D values did not correlate (see main text). The D73 peptide was excluded from power analysis because this mutation impacted peptide loading to MHC. Potency data for this TCR was taken from Kersh et al (7). In the functional experiments, 3.L2 T cell hybridoma cells were incubated with antigen presenting cells pulsed with peptides. Activation was measured by lysis of target cells. P_{40} values (ligand concentration at 40% lysis) of T cell response were given in Figure 4, the corresponding dose response curve was shown in Figure 5. Four data points were included in the analysis and produced $\alpha = 6.8$ (ID 11).

2B4

ID 14 (9) The 2B4 TCR used in this study recognises a moth cytochrome c (MCC) peptide bound to MHC class II molecule I-Ek. Table 2 provides K_D values using SPR at 25°C. The potency of the peptides was determined with T cell hybridomas, stimulated by peptide-pulsed APCs, with activation determined by IL-2 production. For the power analysis we extracted the P_{10} from the dose response curve in Figure 1A. Two data points were available for the power analysis producing an $\alpha = 6.7$ (ID 14).

Revised data for the original mouse TCRs

OT-I

ID 5 (38, 40) Revised affinity data for OT-I TCR was published by Stepanek et al (38). The K_D values were taken from the Table in Figure S1D. Potency data for the same set of peptide variants was measured by Daniels et al (40). Functional experiments were done with pre-selection OT-I double-positive thymocytes. T cell activation was measured by expression of CD69 after incubation with peptide-pulsed antigen presenting cells. EC_{50} values, corrected for small differences in peptide affinity for MHC and normalised to OVA, were given in Figure 1a. Together, these papers provide 5 data points producing α = 2.1 (ID 5).

ID 6 (38, 107) Zehn et al (107) provided additional functional data for OT-I TCR. Potency data is measured by intracellular IFNγ production by OT-I T cells stimulated with peptide pulsed antigen presenting cell. The EC_{50} values, given in table in Supplementary Figure 2C, were normalised to OVA. To calculate the discrimination power, we used K_D values from Stepanek et al (38). The two data points available produced a power of α = 2.0 (ID 6).

ID 7 - 10 (38, 45) Lo et al (45) generated additional functional data for the OT-I TCR. Functional response of $CD8^+$ or $CD8^-$ Jurkat cells expressing the OT-I TCR after stimulation with peptide pulsed antigen presenting cells was measured by CD69 upregulation. The EC_{50} values were provided in Supplementary Figure 7C. K_D values were previously measured by Stepanek et al (38). The study included affinity and potency data for when one of the phosphorylation sites of LAT was mutated. The calculated discrimination power was the same (α = 1.1 for both wild-type LAT (ID 7) and mutated LAT (ID 9) unless CD8 was not present, in which case α= 0.37 (ID 8) or α = 1.4 (ID 10) using Jurkats expressing wild-type or mutated LAT, respectively.

3.L2

ID 12 (84) In this study, the 3.L2 TCR as well as the M15 TCR , a high-affinity TCR engineered from the 3.L2 TCR system, were used, both TCRs bind to murine hemoglobin (Hb 64-76). Table 1 provides K_D values using SPR with at 25°C. Functional data was generated by incubating T hybridoma cells with peptide-pulsed APCs and measuring IL-2 production. We extracted potency values from dose-response curves in Figure 1b and c. Potency values from both TCR systems produces α = 0.37 (ID 12).

ID 13 (41) This paper contain binding and potency data for the 3.L2 TCR interacting with the WT haemoglobin peptide and a panel of altered peptide ligands. Table 2 provides K_D values using SPR at 25°C. The paper does not contain new potency measurement and therefore, we used potency values measured by Kersh and Allen (7) for the power analysis. This dataset produces $\alpha = 3.2$ (ID 13).

2B4

ID 17 (42) This paper contains affinity data for 2B4 TCR binding to its cognate MCC antigen and a set of variant peptides. Table 1 contains K_D values determined by SPR at 25°C. To compare with the original discrimination power, we used the original potency data (9) to produce α = 2.8 (ID 17).

ID 15 - 16 (85) Revised data for 2B4 TCR is provided by Krogsgaard (85). Table 1 provides K_D values measured by SPR at 25°C. For potency measurement, T cells from transgenic 2B4 mice were incubated peptide MHC molecules immobilised on plates, activation was measured by IL-2 production (EC_{50} values were given in Table 1). All ligands were included in the analysis, including those initially labelled as outliers in the publication. The resulting α is 1.2 (ID 16). We also calculated α with affinity data from this study and potency data from Lyons et al (9) (α = 2.2, ID 15).

ID 18 (43) Newell et al (43) studied the 2B4 and the 226 TCRs that bind to MCC. The K_D values were measured by SPR at 25°C and provided in Figure 5D (2B4) and 6B (266). T cell hybridomas were incubated with peptide-pulsed cells and T cell activation measured by IL-2 production. P_{10} (concentration at 10% maximal IL-2 produced by wild-type 2B4) values given in Figure 5C (2B4) and 6 (266). Data for 2B4 produces α = 2.3 (ID 18). The 266 TCR was not included in the analysis, because not enough data points were available.

ID 19- 20 (108) The affinity and potency of the 2B4 and the related 5cc7 TCR, which both interact with MCC, were reported. As before, SPR was used to report K_D values. Functional assays were done with blasted transgenic T cell incubated with peptide pulsed cells. To determine potency, IL-2 production was measured. We extracted both K_D values and EC_{50} values from Figure 4C. Data for 2B4 produced $\alpha = 0.95$ (ID 19) and for 5cc7 produced α = 0.74 (ID 20).

Other mouse TCRs

P14

ID 21 - 22 (86) The mouse P14 TCR that recognises a set of altered peptides from the lymphocytic choriomeningitis virus epitope gp33–41 on murine class I MHC Db. All binding parameters were measured by SPR at 25°C. In functional assays, T cell cytotoxicity, and IFN-γ production of blasted splenocytes from P14 TCR transgenic mice was measured when binding peptide-MHC. Cytotoxicity was measured in a cellular assay, IFNγ production in a plate assay. The EC_{50} is used as potency measurement. All affinity and potency data were provided in Table 2. The α value for this TCR system is 2.1 for cytotoxicity assay (ID 21) and 1.3 for IFNγ assay (ID 22).

B3K506 and B3K508

ID 23 - 26 (109) The MHC-II restricted B3K506 and B3K508 TCRs that recognise the 3K peptide were studied. The K_D values were measured by SPR at 25°C. T cell response was measured by T cell proliferation

and cytokine production after stimulation with peptide-pulsed APCs. All K_D and EC_{50} values were given in Table S1. The B3K506 system produced α = 2.9 (ID 23) and α = 2.4 (ID 24) and the B3K508 system produced α = 2.9 (ID 25) and α = 2.5 (ID 26) for proliferation and TNFα production, respectively.

2C

ID 27 - 29 (110) A panel of TCRs, derived from the murine 2C TCR, that differed in their affinity to the SIYR peptide presented on H-2Kb were used. The K_D values were measured by SPR at 25°C and provided in Table 1. Functional experiments were done with T cell hybridomas with or without CD8 expression. T cells were either incubated with peptides immobilised on plates or with antigen presenting cells pulsed with peptides. For cellular experiments EC_{50} values are given in Figure 3B and D (with and without CD8 respectively), for plate assays in Figure 4B (only CD8 negative data). Most of the ligands have a $K_D < 1$ μM, hence the data points were excluded from the analysis (see inclusion/exclusion criteria in Methods) and therefore, only few data points remained for the power analysis. CD8 negative T cell expressing TCRs stimulated in a plate assay produced $\alpha = 0.12$ (ID 27), however in the cellular assay TCRs binding to the antigen with a $K_D > 1$ were not activated in CD8 negative T cells (no data points to calculate α) (ID 28). TCRs in CD8 positive T cells stimulated in the cellular assay produce $\alpha = 0.66$ (ID 29).

ID 30 (89) The 2C high affinity TCR and variants thereof binding to the QL9 and the altered QL9 peptide F5R were studied. The K_D values were measured by SPR at 25°C. Functional data was generated with T cell hybridomas stimulated by peptide-pulsed APCs with T cell activation assessed by IL-2 production. K_D and EC_{50} values were taken from Table 1. K_D values below 1μM were excluded from our power analysis. This data produces α = 2.7 (ID 30).

ID 31-32 (90) The authors report binding and functional responses of high-affinity 2C TCR variants interacting with SIY peptide on MHC Kb and QL9 peptide on Ld. In total, 8 different TCR/pMHC ligand pairs were included. The K_D values were measured by SPR at 25°C and provided in Table 1. K_D values lower than 1 μM were excluded from the analysis. Functional assays were done with T cell hybridoma with and without CD8 expression with T cell activation assessed by IL-2 production in response to peptide-pulsed APCs. We extracted potency values as P_{50} from dose response curves in Figure 3. TCR variants m6 and m13 when binding to SIY-Kb showed no activation ($P_{50} > 100\mu$M). The calculated discrimination power is α = 4.7 for CD8 positive (ID 31) and α = 6.5 for CD8 negative T cells (ID 32).

Not included (49) This study provided binding and affinity data for the 2C TCR with and without CD8. However, when applying our inclusion/exclusion criteria only a single data point was available and therefore, we were unable to calculate α. The reason is that only few interactions were measured by SPR and the majority of these produced K_D values below 1 μM.

42F3

ID 33 (91) The 42F3 TCR recognises the class I MHC molecule H2-Ld presenting the peptide p2Ca. The K_D values were measured by SPR at 25°C and potency data (EC_{50} of of IL2 production after cellular

stimulation) were taken from Table 1 and Supplementary Figure 3C. The resulting α is 0.15 (ID 33).

Gp70 (AH1)-specific TCR

ID 34 (111) The TCR used in this study recognises the AH1 peptide which is derived from the endogenous retroviral protein gp70(423-431), a MHC class I restricted tumor-associated antigen. The authors used a set of AH1 variants with optimised affinities. The K_D values were measured by SPR at 25°C and provided in Figure 1B. Functional data was generated with a T cell line incubated with peptide-pulsed APCs. EC_{50} values of a proliferation assay are provided in Figure 2B. The calculated discrimination power was $\alpha = 5.2$ (ID 34).

Other human TCRs

1G4

ID 35 (82) The 1G4 TCR used in this study binds the NY-ESO-1 (157-165) peptide loaded on MHC class I HLA-A2. The authors generated a panel of TCRs derived from the human 1G4 TCR that bind with higher affinity than the wild type TCR. The K_D values were measured by SPR at 25°C and provided in a table in Figure 1A. Potency was measured with a cytotoxicity assay and we extracted the mean EC_{50} values from Figure 5E. A decrease in potency was observed for TCRs with an affinity of K_D ¡ 1 μM, which were excluded as per our exclusion criteria (see Methods). This data produced $\alpha = 0.67$ (ID 35).

ID 36 (112) Here, TCR–peptide–MHC binding parameters and T cell function was investigated with a panel of 1G4 TCR variants binding to the the NY-ESO-1 peptide. The K_D values were measured by SPR and provided in Table 1. The functional response of T cells was determined in a cytotoxic T cell assay. We extracted the mean EC_{50} values from Figure 4B. Data points with $K_D < 1\mu$M are excluded from the power analysis. The resulting α is 0.69 (ID 36).

ID 37 - 38 (10) Here, the interaction between 1G4 TCR binding a set of variant NY-ESO-1 (157-165) peptides on MHC class I was studied. The K_D values were measured by SPR at 37°C. The potency was determined by IFNγ production of T cell after stimulation by plate-immobilised pMHC or cytotoxicity by peptide-pulsed T2 APCs. The 1G4 TCR clone was used for both experiments. All affinity and EC_{50} values were given in Table S1. Discrimination power α for the 1G4 system is 0.6 (IFNγ, ID 37) and 1.6 (Cytotoxicity assay, ID 38).

1G4 and G10

ID 39 - 40 (53) Experimental data was generated with the 1G4 and G10 TCR clones binding to a panel of peptide variants. The 1G4 TCR recognises the NY-ESO-1 antigen and the G10 TCR recognises the HIV gag p17 antigen in the context of MHC class I HLA-A2. The K_D values were measured by SPR at 37°C. Potency was determined by measuring IFNγ production in response to plate-immobilised recomvbinant pMHC. All

K_D and EC_{50} values were given in Table S1 and S2. For the 1G4 system we found α = 0.55 (ID 39) and for the G10 system we found α = 0.95 (ID 40).

1E6

ID 41-42 (75) The MHC-I restricted 1E6 TCR reactive to preproinsulin (INS) and variants were studied. The K_D values were measured by SPR at 25 and 37°C and provided in Figure 2. All K_D values lower than 1μM were excluded from the power analysis (see Methods). Functional assays were done with primary T cells responding to peptide-pulsed APCs and target cell lysis was measured for T cell activation. The EC_{50} was determined from the data in Figure 2K. We calculated α = 1.1 for K_D values measured at 25°C (ID 41) and α = 1.2 for K_D values measured at 37°C (ID 42).

A6

ID 43 -44 (94) The A6 and engineered variants recognising the Tax or HuD peptides were used. The K_D values were measured by SPR at 25°C and provided in Figure 1A. T cell activation in response to peptide-pulsed APCs was assessed by CD107a expression and IFNγ production. Potency data was extracted as P_{20} for CD107a assay from dose response curve in Figure 4C and as P_{10} for IFNγ assay from dose response curve in Figure 5A. Data point with $K_D < 1\mu$M were not included in the power analysis. The resulting α is 2.0 (ID 43) and 2.2 (ID 44) for CD107 and IFNγ readout, respectively.

Gp100-specific TCR (Melanoma)

ID 45-46 (96) Seven TCRs specific to human melanoma gp209–2M epitope (modified from gp100 (209-217)) were isolated from patients vaccinated with gp209– 2M. The K_D values of these TCRs measured by SPR at 25°C was provided in Table 1. Functional activity was determined by IFNγ production and ERK phosphorylation of transduced $CD8^+$ splenocytes mixed with peptide-pulsed APCs. Potency values were extracted from Figure S3A and C as P_{10}. The L2G2 TCR, which appeared as an extreme outlier showing the highest potency despite having the lowest affinity, was excluded from the analysis. This data point is shown in the plots as an open circle and including it would have further reduced the estimates α. The calculated powers were α = 1.3 for IFNγ production (ID 45) and α = 1.2 for ERK phosphorylation assay (ID 46).

ID 47 -48 (97) T cell responses of a TCR specific to melanoma epitope gp100(280–288) were studied using a set of altered peptides. The K_D values were measured by SPR at 25°C and provided in Table 2. Functional assays used gp100 TCR-transduced CD8+ T-cells stimulated by peptide-pulsed APCs with T cell activation assessed by cytotoxic lysis and MIP-1β production. We extracted the potency data as P_{10} from dose response curves in Figure 6. The resulting α values were 2.3 (lysis assay, ID 47) and 3.6 (MIP-1β production, ID 48).

14.3.d

ID 49 - 50 (98) T cell responses were measured using variants of the Staphylococcus enterotoxin C3 (SEC3) super antigen. In addition, binding of a panel of mutated variants of the antibody F23.1 were also used. The K_D values of SEC3 were measured by SPR and provided in Table 1. The K_D values of the antibodies were provided in Table 1 of different publication (99). T cell hybridomas, containing a NFAT-GFP expression cassette, were stimulated with SEC3 or antibody molecules immobilised onto plate surfaces to observe functional responses. We extracted all potency values as EC20 from Figure 4. According to our exclusion criteria (see Methods), we did not include any data point where $K_D < 1$ μM. The remaining data points generated with the SEC3 variants produced $\alpha = 0.81$ (ID 49) and with the F23.1 antibody variants produced $\alpha = 0.66$ (ID50).

TCR55

ID 51 (73) This study used TCRs specific for HLA-B35-HIV(Pol448–456) binding to a set of variant peptides. The K_D values were measured by SPR at 25°C. T cell activation after stimulation with peptide pulsed on APCs was measured by CD69 expression. All K_D and EC_{50} values were given in Figure S5C. We calculated $\alpha = 0.19$ (ID 51).

ILA1

ID 52 - 57 (51) The MHC-class I restricted ILA1 TCR is specific for the human telomerase reverse transcriptase (hTERT) epitope ILAKFLHWL (hTERT540-548). The K_D values were measured by SPR at 25°C and provided in Table 1. Three different assays were used to measure T cell activation: Degranulation assay, CD107a expression, and IFNγ production. Each assay was performed using APCs expressing either WT MHC or CD8-null MHC which cannot bind CD8. Potency values for degranulation were given in Table 1, CD107a and IFNγ potency data was extracted from dose response curves in Figure 7. For potency data measured with wild-type (WT) and CD8 null MHC respectively, we calculated an α of 1.5 (WT, ID 52) and 2.5 (CD8 neg., ID 52) for degranulation, 2.2 (WT, ID 54) and 3.6 (CD8 neg., ID 55) for CD107a, and 2.2 (WT, ID 56) and 3.2 (CD8 neg., ID 57) for IFNγ production.

ID 58 - 61 (100) The ILA1 TCR was studied interacting with peptide variants. The K_D values were measurred by SPR at 25°C and provided in Table 1. T cell activation was measured by peptide-pulsed APCs and dertermined by MIP-1β, IFNγ, TNFα, and IL-2 production using intracellular cytokine staining. The potency values were read of as P_{50} from the dose response curves in Figure 2. Authors suggested that the TCR shows a plateau at K_D values ¡ 5 μM. Therefore we decided to exclude K_D values ¡ 5 μM from the power analysis to avoid underestimating the discrimination power α. The data produces α = 1.4 (ID 58), 0.77 (ID 59), 0.97 (ID 60) and 1.1 (ID 61) for MIP-1β, IFNγ, TNFα and IL-2 production respectively.

NY-ESO-1(60-72)-specific TCR

ID 62 (101) Four TCRs binding to the tumorigenic antigen NY-ESO-1(60-72) were obtained from patients with melanomas expressing NY-ESO-1. The K_D values were measured by SPR 25°C and given in Figure 2C. Functional response of TCRs to exogenous peptide stimulation was assessed by measuring IFNγ production of T cells incubated with NY-ESO-1-expressing melanoma cells. We extracted EC_{50} values from dose response curves in Figure 1F. We calculated $\alpha = -0.59$ (ID 62).

Gliadin-specific TCRs (Celiac disease)

ID 63 (102) Seven DQ8-glia-a1-restricted T cell receptors isolated from celiac disease patients were characterised for their binding affinity to a-I- gliadin and their functional response. The K_D values were measured by SPR at 25°C and provided in Figure 2 and S5. T cell activation was assessed by proliferation in response to peptide-pulsed APCs. We extracted P_{20} values from the dose-response curves in Figure 1 (Black curve Q-Q). We calculated an α = 0.83 (ID 63).

LC13

ID 64 - 67 (52) The LC13 and SB27 TCRs were studied using an alanine scan. The K_D values were measured by SPR and provided in Table S2. T cell activation was measured using Jurkat T cells expressing the TCR with CD69 and cytoxicity assessed in response to peptide-pulsed APCs. Figure 1C and 1D showed the dose response curves for CD69 upregulation for either CD8 positive or CD8 negative cells. We extracted the P_{30} as potency measure. EC_{50} of cytotoxicity assay was given in Figure 2 for LC13 and Figure S2 for SB27. Potency values from CD69 produced α = 1.9 (ID 64) for CD8 positive cells and α =7.8 (ID 65) for CD8 negative cells. Lysis assays produced α = 4.1 (ID 66) for the LC13 and α = 0.11 (ID 67) for SB27 TCR.

HIV-Gag293-specific TCRs

ID 68 (103) TCRs specific to HIV Gag293 protein were isolated from patients infected with HIV. The K_D values were measured by SPR and provided in Table 3. T cell activation was assessed using TCR-transduced J76 cells measuring CD69 expression in response to peptide-pulsed APCs. We extracted the mean EC_{50} values from Figure 6D. We calculated $\alpha = 1.0$ (ID 68).

MEL5

ID 69 (104) The MEL5 and MEL187.c5 TCRs were studied that bind the MART-1 antigen and variants thereof. The K_D values were measured by SPR at 25°C and provided in Table 1. T cell activation was measured by MIP-1β production in response to peptide-pulsed APCs. We extracted potency values as P_{50} from dose response curves in Figure 2 and S1. Because responses to peptides were measured in separate experiments, potency data is normalised to wild type peptide. This produced $\alpha = 2.3$ (ID 69).

ID 70 (105) The MEL5, MEL187.c5, DMF4, and DMF5 were studied that recognise the MART-1 antigen. Two overlapping peptides were used: nonapeptide MART-1(27-35) and decapeptide MART-1(26-35). The K_D values were measured by SPR at 25°C and provided in Table 1. T cell activation was assessed using primary human T cells responding to peptide-pulsed APCs with MIP-1β used as a marker of T cell activation. We determined P_{30} directly form does response curves in Figure 1A. Data produced $\alpha = 4.5$ (ID 70)

Other (non-TCR) surface receptors

Cytokine receptors

ID 1-2 (55) Engineered IL-2 variants with increased binding affinity for the interleukin-2 (IL-2) receptor subunit β (IL-2Rb) were studied. The K_D values for IL-2 variants to IL-2Rβ are given in Supplementary Figure 3 and determined by SPR at 25°C. As only the affinities to a single subunit were varied between ligands, potency was plotted over these K_D values. Functional experiments were performed with either CD25 negative human Natural Killer cells or CD25 negative murine T cells. We extracted the EC_{50} values as a measure of potency from dose-response curves in Figure 3a and 3e. We calculated α = 0.55 (ID 1) for experiments done with Natural Killer cells and α = 0.74 (ID 2) for T cells.

ID 3-6 (56) The relationship between the interaction of interleukin 13 (IL-13) with its cytokine receptor and the resulting downstream cellular responses were investigated. A panel of IL-13 variants with a range of binding affinities for the receptor subunit IL-13Ra1 was generated. Binding affinities of these ligands were given in a table in Figure 2C. Here, only the affinity for the α subunit of the receptor dimer was varied and therefore, we plotted potency over these K_D values. Functional responses of binding were determined by measuring STAT6 phosphorylation, CD86 and CD209 production, and proliferation after receptor stimulation. We extracted EC_{50} values for pSTAT6 from Figure 5B. To avoid extrapolating potencies, ligands with EC_{50} larger than highest concentration used in the dose-response (in Figure 5A) were excluded. The mean proliferation EC_{50} values were taken from Figure 5G. CD86 EC_{50} values were extracted from dose response curve in Figure 5H, CD209 EC_{50} values from the dose response curve in Figure S7C. EC_{50} values for CD86 and CD209 extracted from the dose response curves did not exactly match EC_{50} values given in Figure S7 D and E, but both values resulted in similar α values. The α values calculated for the IL-13 receptor are 0.47 (ID 3), 0.39 (ID 4), 0.44 (ID 5), and 0.42 (ID 6) for potency values from pSTAT6, proliferation, CD86, and CD205 assays, respectively.

ID 7-8 (57) Study uses a set of mutated cytokines derived from IFNα2 and IFNω, binding cytokine receptors IFNAR1 and IFNAR2. All binding affinities of mutants normalised to WT are provided in Supplemental Table 2. Because mutations change the affinities to both IFNAR1 and IFNAR2 we calculated an effective binding affinity by multiplying K_D of IFNAR1 with K_D of IFNAR2 (R1xR2). Functional response of cells to cytokine mutants was determined by their antiviral activity in a Hepatitis C Virus Replication Assay, their antiproliferation activity on WISH cells. Mean EC_{50} values normalised to WT obtained from Figure 7A. We calculated $\alpha = 0.71$ (ID 7) for antiviral potency and $\alpha = 1.3$ (ID 8) for antiproliferation potency.

ID 9-11 (58) Study of IFN1 receptor activation with engineered higher-affinity type I IFNs. Affinity constants for peptides to each receptor subunit were measured by SPR. To get the effective K_D we multiplied

K_D of IFN- αR1 bindning with K_D of IFN- αR2 binding (R1xR2) Ligand activity was measured by STAT phosphorylation, antiviral activity and antiproliferation activity. All affinity and EC_{50} values were provided in Table S2. The data produced $\alpha = 0.024$ for STAT1 phosphorylation (ID 9), $\alpha = 0.034$ for antiviral activity (ID 10), and α = 0.50 (ID 11) for the anti-proliferation assay.

ID 12-13 (59) In this study, the authors engineered IL-6 variants with different affinities to the IL-6 receptor subunit gp130. Cytokine gp130 binding kinetics were measured with a switchSENSE chip, binding parameters were given in Supplementary Figure 1D. The influence of IL-6 variants on functional activity of the receptor was determined by the amount of STAT1 and STAT3 phosphorylation at different ligand concentrations. We read off the potency of each ligand as P_{25} directly from dose response curves in Figure 2A and B. We calculated α = 0.54 for pSTAT1 (ID 12) and α = 0.52 for pSTAT 3 (ID 13).

Receptor Tyrosine Kinase (RTK)

ID 14 (61) In this study the effect of three mutated epidermal growth factor on epidermal growth factor receptor (EGFR) was studied. Affinity values of growth factor to receptor were measured with radioactive labelled ligands binding to receptors on cells. Data are given in Table 1. Functional response of cells to ligands was determined by measuring the specific growth rate after stimulation. We extracted the EC_{50} values from dose response curves in Figure 4. This produced $\alpha = 0.55$ (ID 14).

ID 15 - 16 (60) Paper contains data on the c-Kit receptor tyrosine kinase which is activated by the Stem cell factor (SCF). Affinity and functional response of the receptor to SCF variants was studied. Binding parameters were measured by SPR and provided in Figure 1F. Cell activation after stimulation with ligands was determined by the amount of ERK and AKT phosphorylation (pERK and pAKT). We extracted the potency data for each variant as EC_{50} from dose response curves in Figure 2D and 2E. We calculated α = 0.83 (ID 15) and α = 0.88 (ID 16) for pERK and pAKT measurements respectively.

GPCRs

ID 17 -18 (63) The binding parameters of the GPCR adenosine A2A receptor to various agoinist and their functional effects were studied. Association and dissociation rates, and hence K_D values, were determined with a kinetic radioligand binding assay. Functional activity of HEK293 expressing the A2A receptor was measured by detecting cAMP production and changes in cell morphology. The binding data was provided in Table 3 and EC_{50} values from functional experiments were given in Table 4. The discrimination power calculated with cell morphology data is $\alpha = 0.29$(ID 17) and with the cAMP assay produced α = 0.71 (ID 18).

ID 19-20 (62) The M3 muscarinic receptor was studied using a set of agaonist. The binding kinetics were determined with competition binding assay and were provided in Table 1. Agonist potency was measured by guanosine 5'-O- (3-[35S]thio) triphosphate (GTPγS) binding to GαD subunits, and by intracellular calcium levels after receptor stimulation. Potency data measured as EC_{50} values were provided in Table 2. The

resulting power was $\alpha = 0.77$ (ID 19) and $\alpha = 0.55$ (ID 20) for calcium response and GTPγS binding assay, respectively.

ID 21 (64) The CXCR4 receptor is activated by the chemokine CXCL12. In this paper, the interaction of Baclofen and other GABA ligands were tested on their abilities to activate CXCR4. The affinity of ligands to the receptor was measured by back-scattering interferometry and K_D values given in Figure 7. Functional response of oocytes expressing CXCR4 to ligands was determined by measuring the inward currents at different ligand concentrations. EC_{50} values were provided in Table 1. We calculated αD = 0.57 for this system (ID 21).

ID 22 -24 (65) Characterisation of binding properties and potencies of CXC chemokine receptor 3 antagonists. Binding properties of antagonist were determined using kinetic radioligand binding assay. Affinity values were in Table 1 measured for different cell lines. Functional responses after ligand binding were measured guanosine 5'-O-(3-[35S]thio)triphosphate (GTPyS) binding, calcium release, and cellular chemotaxis. All EC_{50} values of assays were given in the text. We calculated αD = 0.72 (ID 22) , 1.1 (ID 23), and 0.56 (ID 24) for calcium release, GTPyS binding, chemotaxis assays respectively.

CARs

ID 25 (106) This study contain affinity and potency data for a CAR binding the ErbB2 surface antigen. The authors generated a series of anti-ErB2 single-chain variable fragments fused to the CD3ζ cytoplasmic domain. The K_D values are reported in Table 1. Functional experiments were done in a plate assay, with ErbB2 immobilised to a surface. Potency of receptors was measured by IFNγ production of T cells after stimulation. We extracted P_{20} values from dose response curve in Figure 4A. The resulting α is 0.52 (ID 25).

ID 26-27 (67) This study characterised a panel of CARs that bind to the ErbB2 surface protein. CARs were constructed by linking the various anti-ErB2 single-chain variable fragments to the CD8αD hinge and transmembrane domain followed by the 4-1BB and CD3ζ intracellular signalling domains. The K_D values were measured by SPR and provided in Table S1. We obtained potency data by using CD107a expression and proliferation assay data in Figure 2A and C to the respective plot dose response curves. P_{50} values were extracted from these plots. The resulting α values are 1.1 for CD107 (ID 26) and 0.64 for proliferation assay (ID 27).

ID 28 (68) Taylor et al (68) developed a synthetic CAR signaling system in which the extracellular domains of the CAR and its ligand antigen were exchanged with short hybridizing strands of DNA. The DNA-CARζ consist of a ssDNA covalently attached to a SNAP tag protein which was fused to a transmembrane domain and the CD3ζ chain. Stands of different length and sequence were designed to vary the affinity of the CAR to the ligand. Binding was measured as the lifetime (τ_{corr}) of single ligand-CAR interactions using microscopy and corrected for photobleaching and provided in Figure 2D. The dissociation rate k_off was calculated from the lifetimes with $k_{\text{off}} = ln(2)/\tau$. To measure T cell responses, ligands, consisting of the complimentary strand of ssDNA, were anchored in planar supported lipid bilayer where they can freely

diffuse. The DNA-CARζ was expressed in TCR negative Jurkat cells. Cell activation after incubation with ligands was measured by phosphorylation of ERK. Potency data was extracted as P_{20} from dose response curves in Figure 2C. This CAR system produced α = 1.2 (ID 28).

BCRs

ID 29-30 (69) The study used the HyHEL10 and D1.3 BCRs, which have a high affinity to the hen egg lysozyme (HEL) and variants thereof. The K_D values were measured by SPR at 25°C and dissociation rates were provided in Table 1. For functional experiments, the ability of B cells to mediate HEL presentation to T cell hybridomas after stimulation with mutant lysozymes was determined by measuring IL-2 production of T cells specific to HEL. We extracted the potency data from dose response curves in Figure 3 and 4 as EC_{50}. The authors described an affinity floor for the B cell receptor when the dissociation rate was below 10^{-4} s^{-1} so that potency did not longer decrease for these interactions. To avoid underestimating α, we did not include these higher affinity ligands in the power analysis. The resulting α values were α = 1.4 for the D1.3 BCR (ID 29) and α = 1.3 for the HyHEL10 BCR (ID 30).

Calculations of sensitivity and discrimination using the kinetic proofreading model

One of the first models to explain the specificity of the TCR is the kinetic proofreading model proposed by McKeithan (18). In this model high specificity is achieved through additional reaction steps between ligand binding and TCR triggering that introduce a delay in the signalling cascade (Fig 6A). Biologically, it is assumed that the delay comes from multiple phosphorylation events on the TCR adaptor protein CD3 and other signalling events of the TCR signalling pathway such as ZAP70 binding. These events are termed the kinetic proofreading steps. Only peptides with a low ligand dissociation rate bind to the TCR for a sufficient length of time to complete all proofreading steps and trigger the downstream pathway. In particular, if the ligand dissociates before TCR triggering, the TCR is rapidly dephosphorylated such that when a peptide next binds to the TCR all the proofreading steps must be repeated. The specificity of the TCR depends on both the number of proofreading steps and the rate at which proofreading steps are completed.

The kinetic proofreading model is formulated as follows. Let L_0 and R_0 denote the initial number of the peptide-MHC ligand and T cell receptors, respectively. Ligand and receptor bind to form a complex C_0 at rate k_{on} and this complex dissociates at rate k_{off}. Additionally, let N be the number of proofreading steps and k_{p} be the proofreading rate. Then the steady state concentration of peptide-receptor complexes in the N-th proofreading step, C_N, is given by

$$C_N = (1+\beta)^{-N}\, C_{\mathrm{total}}, \tag{1}$$

where $\beta = k_{\mathrm{off}}/k_{\mathrm{p}}$ and

$$C_{\mathrm{total}} = \frac{L_0 + R_0 + \frac{k_{\mathrm{off}}}{k_{\mathrm{on}}} - \sqrt{\left(L_0 + R_0 + \frac{k_{\mathrm{off}}}{k_{\mathrm{on}}}\right)^2 - 4L_0R_0}}{2}, \tag{2}$$

is the total number of receptor bound complexes. If $k_{\mathrm{off}}/k_{\mathrm{on}} \ll L_0 + R_0$ the expression for C_{total} simplifies such that $C_{\mathrm{total}} \approx \min(L_0, R_0)$.

To test whether kinetic proofreading is sufficient to explain antigen discrimination we construct two checks to see whether it fulfils the constraints of both sensitivity and discrimination strength. Firstly we let T be the minimum threshold concentration of TCR complexes in the N-th proofreading step needed to initiate a TCR signalling response. Therefore, to check for sensitivity we require that a single ligand interaction with the highest affinity must overcome the threshold of activation. Noting that $\min(1, R_0) = 1$, we can write the sensitivity requirement as the following inequality:

$$C_N = (1+\beta)^{-N} > T. \tag{3}$$

With our empirical equation for the discrimination power $P = 10^C K_D^\alpha$ we can calculate the potency P for a given ligand affinity. Assuming K_D is proportional to k_{off} and P is a ligand concentration needed to activate the TCR L_0, we can rewrite the equation to $L_0 = 10^C k_{off}^\alpha$. The difference in potency between the ligand interaction with the highest affinity $K_{D;1}$ and a ligand with lower affinity $K_{D;2}$ is hence:

$$\frac{L_{0;2}}{L_{0;1}} = \left(\frac{k_{\text{off};2}}{k_{\text{off};1}}\right)^\alpha \tag{4}$$

As we require $L_{0;1}$ to be 1 to fulfil the sensitivity constrain the equation simplifies to $L_{0;2} = \Delta^\alpha$ with Δ being the difference in affinity between the two ligands. Hence a ligand with Δ-fold lower affinity than the highest affinity ligand will need a concentration of $L_{0;2}$ ligands for activation. For the discrimination constraint we require that a ligand with Δ fold less affinity than the highest affinity ligand, needs $L_{0;2}$ or more ligands to overcome the threshold of activation.

The discrimination requirement can be written as the following inequality:

$$C_N = \min(L_{0;2}, R_0)(1+\Delta\beta)^{-N} < T. \tag{5}$$

Both of these constraints must be fulfilled simultaneously in order for the kinetic proofreading model to explain antigen discrimination.

For the simulation of the KP model (Fig 6B) we choose Δ such that $L_{0;2} = 10,000$ according to $\Delta_A = 10000^{1/\alpha}$. As the number of receptors on a cell R_0 is approximately 30,000 choosing $\Delta_L < R_0$ means that the receptors are not saturated with ligands and potency varies linearly with affinity . The final discrimination constraint function is as follows:

$$C_N = 10000(1+10000^{1/\alpha}\beta)^{-N} < T. \tag{6}$$

Parameter sweep for the kinetic proofreading model

In addition to the continuous constraints derived above, in Fig. 6 of the main text we present a parameter sweep of the kinetic proofreading model using discrete stochastic simulations to see for which model parameters both sensitivity and discrimination constraints are satisfied. Our sweep varies the parameters N, the number of KP steps, and $\tau = 1/k_p$, the proofreading time per step. For each pair of parameters (N, τ) we simulate 250 realisations of the kinetic proofreading model using a standard Gillespie algorithm until a termination time of $t = 100$, which is sufficient in order for the model to have reached a steady state. From this ensemble, an average number of receptors in the final (N-th) proofreading step, $\langle C_N \rangle$, is calculated. This ensemble average is compared to the threshold for activation $T = 0.1$.

Testing for both sensitivity and discrimination for each parameter pair (N, τ) requires simulating the model in two different scenarios. The first scenario is with a single ligand and unit dissociation rate, i.e. $k_{\text{off}} = 1$. If the ensemble average $\langle C_N \rangle > 0.1$ then the parameter pair (N, τ) observes sensitivity and is shown as a red asterisk in the panels in Fig. 6. For discrimination we increase the number of ligands to $\Delta_L = 10000$ and increase the affinity of the ligand by $\Delta_A = 10000^{1/\alpha}$, i.e. $k_{\text{off}} = 10000^{1/\alpha}$. If the average number of receptors $\langle C_N \rangle < 0.1$ then discrimination is observed, and the parameter pair (N, τ) is shown as a blue square. Parameter pairs that are shown with both a red asterisk and a blue square observe both sensitivity and discrimination. All stochastic simulations were performed with custom Julia code using the package *DifferentialEquations.jl*.